On Impedance Based RF Dielectric Sensors and Applications in Agricultural Materials

A THESIS
SUBMITTED TO THE FACULTY OF THE GRADUATE SCHOOL
OF THE UNIVERSITY OF MINNESOTA
BY

Joshua D. Braun

IN PARTIAL FULFILLMENT OF THE REQUIREMENTS
FOR THE DEGREE OF
MASTER OF SCIENCE

Dr. Jonathan Chaplin

August 2010

Acknowledgements

I would like to thank my advisor, Dr. Jonathan Chaplin whose guidance and support inspired me to ask the questions.

I would also like to thank the many people who assisted me in my studies and research, especially my committee members. And to the many others who shared their knowledge graciously, thank you.

Dedication

For Beth, whose steadfast encouragement always brings out my best, and for Laura, whose curiosity inspires me.

Abstract

Increasing numbers of commercially available sensors claim to use the dielectric response of grains and other agricultural materials to sense moisture and additional properties. A review of past and current research in this area gives a basis for investigating the efficacy and potential of one such instrument. A variety of materials, including corn, soybeans, wheat, ground feed, and soils were examined. Potential factors for varietal classification within and material type classification between samples was determined to be impractical due to the strong confounding effect of moisture dependence.

Sensor electrode topology was briefly touched on, raising interesting questions about effects of geometry in dielectric sensors. The effect of material presentation was also evaluated for both static and flowing samples. Using continuously flowing samples, several varieties of corn were tested to evaluate existing density independent moisture functions and density functions. The results verified the effectiveness of many functions previously only studied in the microwave range for radio frequency instruments. In addition, a new density prediction function was discovered to have significantly better performance at radio frequencies.

Table of Contents

List of Tables

List of Figures

Disclaimer

Reference herein to any specific commercial products, process, or service by trade name, trademark, manufacturer, or otherwise, does not necessarily constitute or imply its endorsement, recommendation, or favoring by the University of Minnesota nor the author. The views and opinions of authors expressed herein do not necessarily state or reflect those of the University of Minnesota, and shall not be used for advertising or product endorsement purposes.

Introduction

The instrumentation of agricultural systems has been an area of research interest for many decades. In particular, study of the physical properties of products applied to and harvested from fields in production agriculture has proven to be an enticing and fruitful area of research. Grain is bought and sold on the basis of its moisture content and density. Instruments that seek to measure those properties more accurately, with better reliability, and more expediently have been developed over the past decades and have received regulatory approval for trade. However, despite improving and expediting the commercial handling of grain, these devices rely on undersized samplings of a much larger volume of product (on the order of 25ppm). On-line sensors which measure a significantly larger proportion of the product in real-time have started to see application. One such commercially available instrument was developed to sense moisture and density of whole kernel corn (Greer, 2002). This study focuses on the efficacy of real time density and moisture sensors and examines applications for a variety of agricultural material.

Background

Dielectric materials provide an interesting media for electric field interactions. These interactions have been studied intensely over the past century leading to a wide range of applications. In particular, dielectric interactions have been studied for the purposes of developing instrumentation for measurement of granular solids. The following review identifies the underlying principles behind these types of measurements and summarizes relevant literature in the field.

Complex Permittivity

Complex permittivity is the central property among examination of dielectrics. This parameter indicates the ability of a given material to store energy imparted by an electric field as well as its efficiency in storing the energy. Permittivity (ε) can be expressed as a function of the permittivity of free space, ε_0. This quantity is known as relative permittivity:

$$\varepsilon_r = \frac{\varepsilon}{\varepsilon_0} \tag{1}$$

The relative complex permittivity (ε_r^*) can then be expressed as:

$$\varepsilon_r^* = \varepsilon_r' - j\varepsilon_r'' \tag{2}$$

The two terms of the complex permittivity are represented by the dielectric constant ε_r', which is the ability of a material to elastically store energy from an electric field, and the dielectric loss factor ε_r'', electric field energy dissipated by the material. These two terms can also define the loss tangent:

$$\tan(\delta) = \frac{\varepsilon_r''}{\varepsilon_r'} \tag{3}$$

which has been shown to be a useful measure to remove permittivity's dependence on density (Trabelsi et al., 1998).

Polarization

There are several mechanisms for storing energy in a dielectric material based on polarization of individual atoms and molecules by the presence of an electric field. Mechanisms include electronic polarization, occurring through the deformation of the

electron cloud surrounding individual atoms, and rotational polarization resulting when polar molecules are reoriented by an electric field (Griffiths, 1981; Von Hippel, 1954).

Most study of dielectric materials focuses on molecular polar dipoles which can have relatively large and distinctive dipole moments. A dipole's polarity is measured in Debyes (C m) indicating the strength of a charge and what distance it is displaced. In particular, water, which has a 104 degree angle between its hydrogen atoms, has a particularly strong moment of 1.84 Debyes (6.14×10^{-30} C m).

Frequency Dependence

The complex permittivity of dielectrics is a frequency dependent property. Debye (1929) found that for materials with a single relaxation method, the complex permittivity of a material could be represented as a function of the response dielectric constant at low frequencies (ε_S), at high frequencies (ε_∞), a relaxation time constant (τ), and the frequency (ω). The result, known as the Debye equation:

$$\varepsilon^* = \varepsilon_\infty + \frac{\varepsilon_S - \varepsilon_\infty}{1 + j\omega\tau} \tag{4}$$

can be separated out into the real (5) and imaginary (6) terms, dielectric constant and loss. (Both ε_S and ε_∞ are assumed to be real.)

$$\varepsilon_r' = \varepsilon_\infty + \frac{\varepsilon_S - \varepsilon_\infty}{1 + \omega^2\tau^2} \tag{5}$$

$$\varepsilon_r'' = \varepsilon_\infty + \frac{(\varepsilon_S - \varepsilon_\infty)\omega\tau}{1 + \omega^2\tau^2} \tag{6}$$

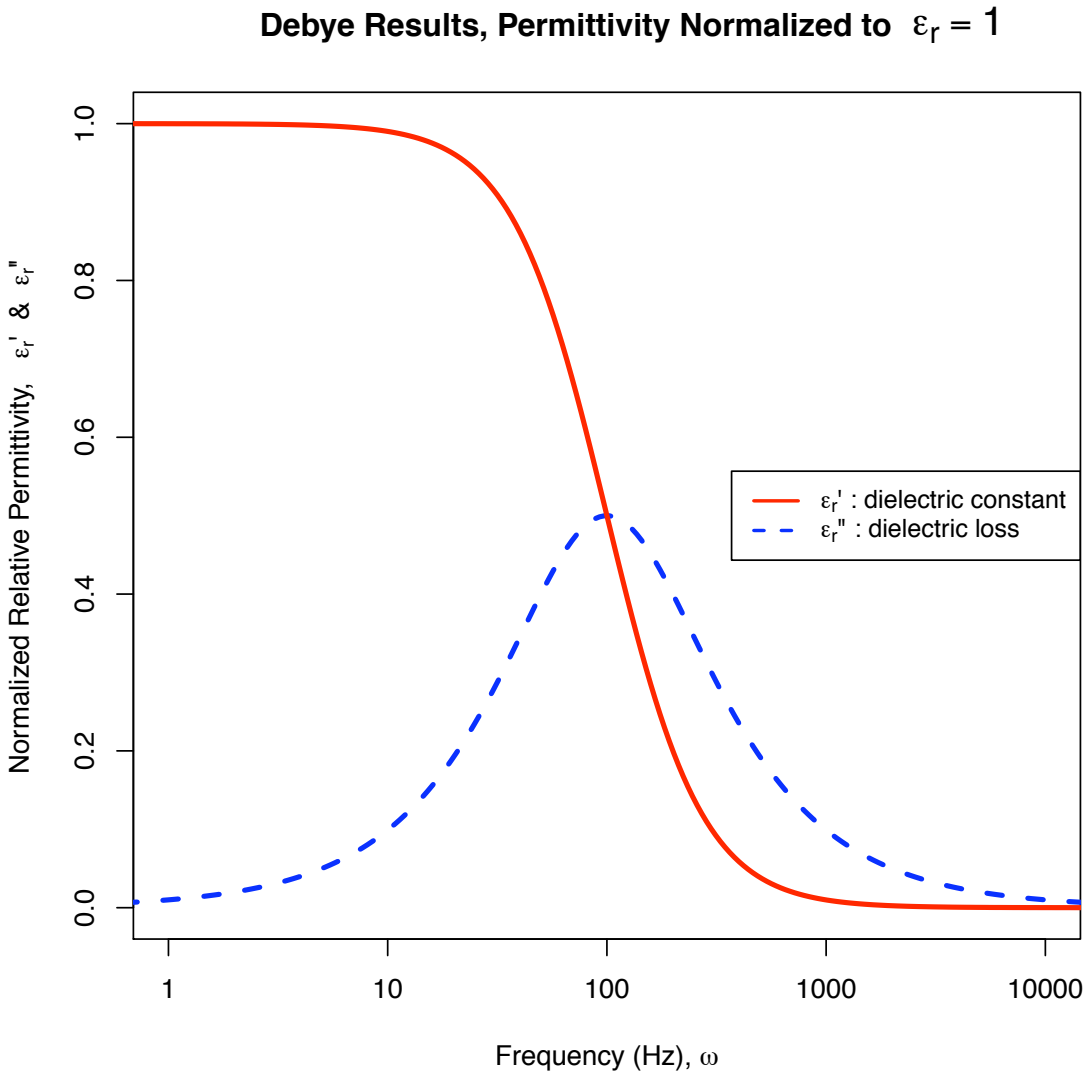

Figure 1: Debye equation results for relative dielectric constant and loss.

Figure 1 shows a normalized graph of the dielectric constant and loss factor as a function of frequency for a material with a single relaxation method (e.g. molecular dipole polarization). The behavior of the complex permittivity at its frequency limits gives a good indication to the general behavior of dielectric relaxations. A maximum permittivity will be obtained at the static limit ($\omega = 0$Hz). As the frequency rises, a monotonic decrease in dielectric constant is observed until the high frequency limit

($\omega \to \infty$) is reached. For the dielectric loss, a maximum, located at the midpoint between static and high frequency dielectric constants, is achieved when the relaxation frequency ω and the relaxation constant τ are equal.

Lumped Element Model

The Debye equation can be derived from the electrical response of an ideal RC circuit, in which two capacitors are wired in parallel, one with an additional series resistance. Von Hippel states that this approximation is appropriate due to the dominating friction polar molecules experience in a solid material that allows the simplification of the resonator model (LRC) to the RC circuit in Figure 2 with impedance (Von Hippel, 1954):

$$Z = \left(j\omega C_1 + \frac{1}{R_2 + \frac{1}{j\omega C_2}} \right)^{-1} \tag{7}$$

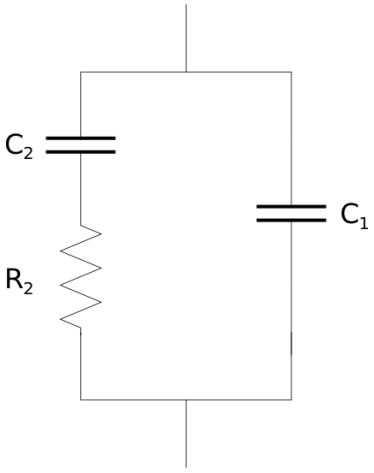

Figure 2: Analogous RC circuit for polarized molecular rotor in solid material.

If the capacitor C_2 is charged to a voltage V_0 and allowed to discharge, the following response is observed over time:

$$V_2 = V_0 e^{\frac{-t}{R_2 C_2}} \tag{8}$$

The discharge time constant can be defined as $\tau \equiv R_2 C_2$. Given a parallel plate chamber with open air capacitance C_0, and impedance $Z = 1/j\omega\varepsilon^* C_0$ the impedances in Figure 2, yields a permittivity of:

$$\varepsilon^* = \frac{C_1}{C_0} + \frac{C_2}{C_0}\frac{1}{1 + j\omega\tau} \tag{9}$$

When the static and high frequency cases are examined, the analog between the RC circuit and Debye's model become apparent. For the high frequency limit the permittivity becomes:

$$\varepsilon_\infty = \frac{C_1}{C_0} \tag{10}$$

and for the lower static limit (ω = 0Hz) it is:

$$\varepsilon_S = \frac{C_1}{C_0} + \frac{C_2}{C_0} \tag{11}$$

giving a generalized form of:

$$\varepsilon^* = \varepsilon_\infty + \frac{\varepsilon_S - \varepsilon_\infty}{1 + j\omega\tau} \tag{12}$$

This analog can be used to build more complex cases and allows for the approximation of the behavior of a particular instrument.

Basic Dielectric Properties of Grain

Dielectric based measurement of moisture in grains has been used for nearly 100 years with evidence in patent filings from as early as 1929 (Heppenstall, 1929). Nearly all of the work characterizing the quantitative dielectric properties of granular media has occurred in the last 50 years. The vast majority of study has been on agricultural materials, specifically grains and oilseeds with the goals of improving quality and automation in agricultural processes (Nelson, 1981; Nelson, 2006). Most of this research has focused on wheat and corn, with soybeans and other small grains studied to a lesser extent. In studies where alternating current based instrumentation was used, the frequency of measurement ranged from 250Hz to more than 12GHz. Moistures studied were dependent on seed type and ranged from 2% wet basis moisture to more than 50%. Over these ranges of frequency and moisture some generalizations about the dielectric properties have been made. Increasing moisture in tested seeds resulted in monotonically increasing dielectric constants (ε_r'). These studies also indicated that ε_r' either remained constant or decreased with increasing measurement frequency. The correlation between the dielectric loss factor (ε_r'') and either moisture or frequency could not be generalized. Figure 3 illustrates the frequency and moisture dependence for both dielectric constant and loss factors over ranges of each for hard red winter wheat (ASABE, 2005). Over the span of research, numerous studies cite several reasons for the irregular behavior of the dielectric loss factor (Nelson, 1981; Funk et al., 2007). The most recent findings indicate that the dielectric loss' large values and steep slopes come not from dielectric relaxation and dispersion as discussed above (polarization) which has been attributed to water bound within the grains. Rather, Funk states that these effects are due to conductivity.

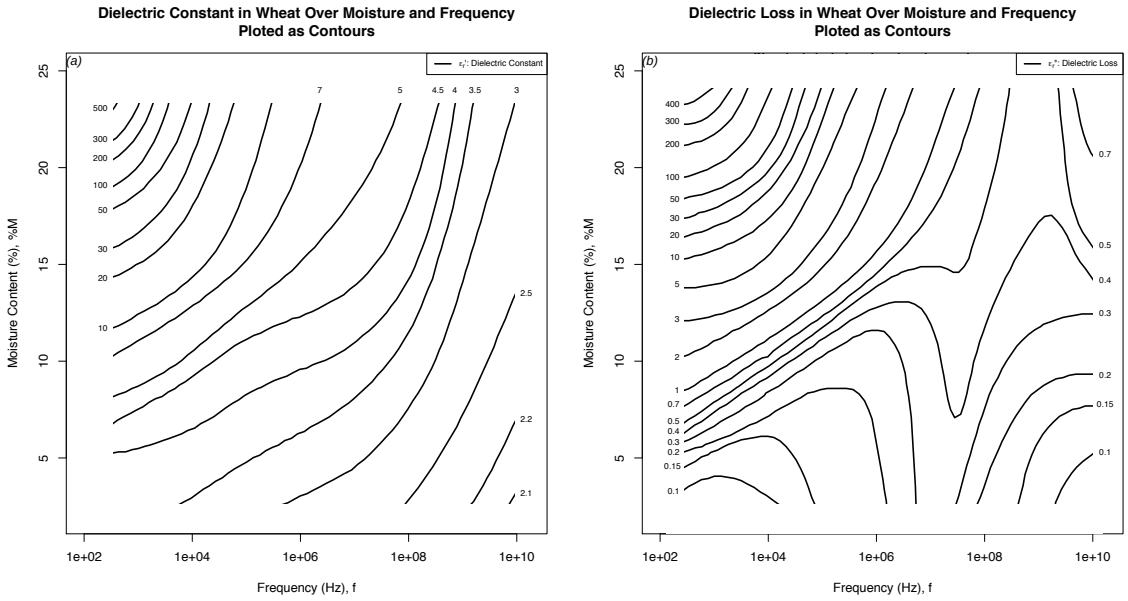

Figure 3: Dielectric constant (a) and loss factor (b) measured over frequency and moisture for hard red winter wheat (Nelson, 1981).

Conductivity Effects

Grimnes and Martinsen (2000) explain these effects as types of interfacial polarization, that is, a collection of charge at boundaries within a measured sample. A parallel-plate cell filled with a sample material and pulsed with alternating current illustrates the simple case of electrode polarization. During each half cycle of sample excitation, the electric field will create a charge carrier build up at the electrode's interface given the right conditions. One of these conditions is the relative resistance between the sample cell electrodes and the sample material (contact resistance) and the internal resistance of the sample material. If the contact resistance is large relative to the internal resistance, charge carriers will migrate. As the electric field oscillation frequency becomes very low (relative to the time it takes these charge carriers to move), many charge carriers can accumulate at the electrodes. This charge movement appears as

an increase in permittivity despite having no link to the physical dielectric values of the material being examined.

More complex are Maxwell-Wegner relaxations in dielectrics. In granular media, each boundary between granules can become an electrical interfacial boundary (as above) with varying boundary resistances due to the non-uniformity of most samples. Maxwell-Wegner relaxation exhibits behavior similar to the Debye result (see Figure 3) where the contribution to the dielectric constant decreases with increasing frequency. The dielectric loss factor is also maximized where the dielectric constant is changing at the greatest rate, going to zero at very low and very high frequencies. Funk concludes that conductivity effects are particularly difficult to model due to the complexity of interactions within granular materials and the effects' large moisture dependent variations (Funk et al., 2007).

Dielectric Mixtures

Dielectric measurements of single granules have obtained dielectric constant and loss factor properties for a number of materials (Lawrence and Nelson, 2000; Nelson et al., 1992). Extrapolating the single granule measurements, studies have modeled the macroscopic behavior observed in measurements of granular media in bulk (Nelson, 2001; Hilhorst et al., 2000; Nelson, 2005). Most frequently the mixing is done in air, but other studies have examined individual granule degradation by modeling multiple ground fractions in addition to the whole material and air (Al-Mahasneh et al., 2001). Nelson (2001, 2005) has shown repeatedly that the best models are the complex refractive index mixture equation:

$$\varepsilon^{1/2} = \upsilon_1 \varepsilon_1^{1/2} + \upsilon_2 \varepsilon_2^{1/2} \tag{13}$$

and the Landau and Lifshitz, Looyenga equation:

$$\varepsilon^{1/3} = \upsilon_1 \varepsilon_1^{1/3} + \upsilon_2 \varepsilon_2^{1/3} \tag{14}$$

where ε, ε_1 and ε_2 are the complex dielectric constants of the mixture, the first and the second materials, and υ_1 and υ_2 are the respective volume fractions. It has been shown that the error performance of the Landau and Lifshitz, Looyenga equation is superior. Nelson also suggested a simplification for the special case of an air-particle mixture, (the typical case) which allows density corrections of permittivities to be made based on a known permittivity and density pair (Nelson, 2005). The extrapolated complex dielectric constant for an air-particle mixture can be represented by:

$$\varepsilon_b = \left\{ \left(\varepsilon_a^{1/3} - 1 \right) \frac{\rho_b}{\rho_a} + 1 \right\}^3 \tag{15}$$

where ε_a is the known complex dielectric constant with density ρ_a and ε_b is the predicted complex dielectric constant at the new density ρ_b.

Density Dependence

Much effort has gone into attempts at either removing the effect of density on the correlation between complex permittivity and moisture or removing moisture's effect on the correlation between complex permittivity and density (Funk et al., 2007; Lawrence and Nelson, 2000; Sacilik et al., 2007; Kraszewski et al., 2000; Trabelsi et al., 2001b). Most recently the Landau and Lifshitz, Looyenga mixture equations have been implemented by Funk as part of a unified moisture algorithm for sensing grain moisture

(Funk et al., 2007). Trabelsi developed another density independence model utilizing the relationship between attenuation and phase shift at microwave frequencies (Trabelsi et al., 1998; Trabelsi et al., 2001b; Trabelsi et al., 1999a). This equation ultimately yields a moisture calibration expressed as a function of dielectric constant and loss factor:

$$\Psi = \sqrt{\frac{\varepsilon''}{\varepsilon'\left(a_f \varepsilon' - \varepsilon''\right)}} \tag{16}$$

where a_f is the frequency dependent coefficient, determined by the slope of the plot ε''/ρ against ε'/ρ. Ultimately, development of fitting algorithms for density correction and determination continues to be an area of active research due to calibrations that are too restrictive and do not generalize well.

Hydrogen Bonding and Temperature Dependence

In addition to density dependence, research has shown that the complex dielectric constant depends on temperature at which a material is measured. Funk cites several authors and develops a framework for understanding this behavior at a molecular level (Funk, 2001). This framework depends on the concept of free and bound water. Many authors have discussed the concept of free and bound water. The BET model defines bound water as molecules where hydrogen bonding has been established between the water and a polar site on the host material. Frequently carbohydrates and proteins provide these sites in grains. This type of binding is also referred to as monolayer water; the water molecules no longer have the freedom to create a lattice structure when cooled below 0°C. In contrast, free water continues to freeze at 0°C, filling capillary spaces of the material and continuing to allow for ionic conduction as it still functions as a solvent.

A further extension of the BET model involves decreased strength in binding forces for water molecules beyond the first layer (monolayer) leading to a range of binding energies for varying saturations of water within a material. These ranging binding energies are a key driver in dielectric behavior of materials with significant fractions of water.

A quantitative study of water adsorption into grain gives credence to this model (Trabelsi and Nelson, 2007). Hilhorst developed a relationship between relaxation frequency and the required change in Gibbs free energy (Hilhorst, 1998). A further extension of kinetic rate theory indicates that this relation can be quantized by correlating the relaxation frequency (f_r) to the probability of breaking a hydrogen bond that restrains a water molecule during a single relaxation period ($\tau = 1/2\pi f_r$) (Funk, 2001). The relationship is:

$$f_r = \frac{kT}{2\pi h} e^{\frac{\Delta G}{RT}} \tag{17}$$

where ΔG is the change in Gibbs free energy, h is Planck's constant, k is Boltzmann's constant, T is the temperature in Kelvin, and R is the gas constant. The reforming of these bonds occurs very rapidly (~0.1ps) relative to most instrumentation (Kraszewski, 1996). This indicates that the relaxation time for water is driven primarily by molecules waiting for their bonding energy to be overcome. Further derivation by Hilhorst shows that only the portion of Gibbs free energy due to the molar activation enthalpy need be considered (Hilhorst, 1998). That is $\Delta G \approx \Delta H$. Continued development of this relationship yields a relaxation frequency of a bound species of water, f_r to be proportional to the relaxation frequency of free water, f_{r0}. That is:

$$f_r = f_{r0} e^{\frac{\Delta H_0 - \Delta H}{RT}} \quad (18)$$

where ΔH_0 (the molar activation enthalpy of free water) can be estimated to be 20.5kJ/mol and f_{r0} to be 17GHz. A lower bound to the relaxation frequency of 10kHz can be determined by substituting the empirically determined value of 55kJ/mol for the activation enthalpy of ice. Hence, hydrogen bonding plays a significant role in the exact relaxation frequencies and thus the dielectric constants of materials with significant fractions of water. Through this relation, temperature will also affect the dielectric constant by increasing the relaxation frequency over increasing temperature. This effect is mitigated by the increasing disorder of a system at higher temperatures and under certain circumstances causes a decrease in the dielectric constant. These effects are illustrated by Funk in Figure 4. Temperature dependence is primarily influenced by the excitation frequency's proximity to the relaxation frequency. Near the relaxation frequency where the dielectric loss is significant, the effect of temperature is positively correlated to the complex permittivity. Elsewhere, the effect is generally negatively correlated. Research has confirmed these generalizations (Funk, 2001; Funk et al., 2007; Trabelsi and Nelson, 2004).

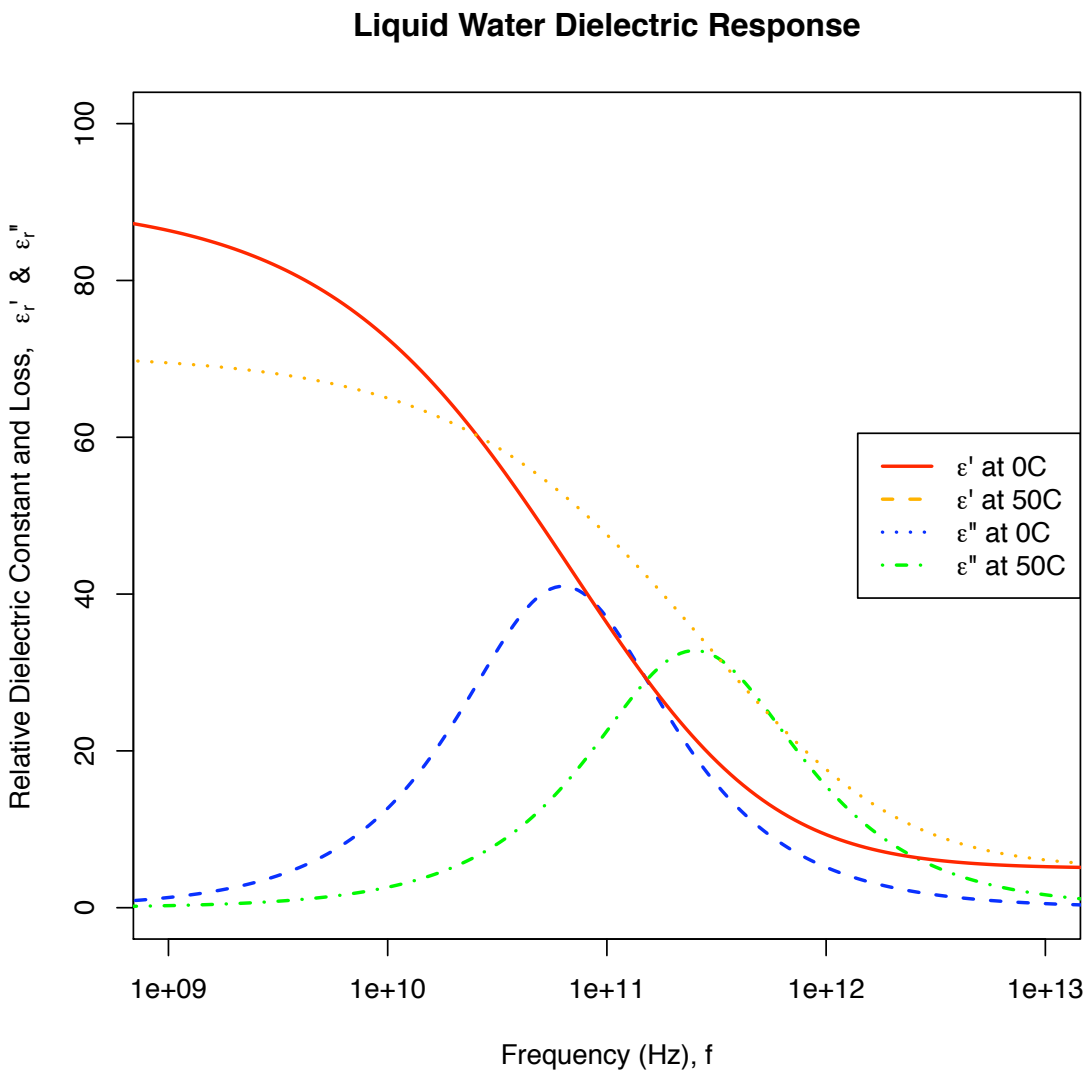

Figure 4: Liquid water dielectric constant and dielectric loss at 0°C and 50°C (Funk, 2001).

Instrumentation for Dielectric Measurement

Many sources discuss the implementation of devices designed to measure the complex permittivity of materials (Nelson, 2006; Funk et al., 2007; Lawrence and Nelson, 2000; Kraszewski et al., 2000; Trabelsi et al., 2001b; Nelson and Bartley, 2000; Nelson, 1999; Trabelsi et al., 2001a; Nelson, 1992). Such devices have been designed to

measure properties of single granules of seeds as well as measurement of material in bulk.

Two approaches have been used throughout the research: an impedance technique based on the measure of relative capacitance and wave propagation measurement. The classic example of the former is a test cell designed in the form of a parallel plate capacitor with an initial dielectric of air. The measurement is completed when a sample material replaces the air in the test cell and a change in capacitance is recorded. This technique saw formative development from Nelson with the creation of a Q-meter that quantified much of the earliest grain dielectric measurements (Nelson, 1999). The complex dielectric constant is a simple ratio between the complex capacitance of the filled test cell and the air filled (empty) test cell. Any additional contributions to the capacitance of the air filled test cell, easily measured when empty, must be subtracted from all measurements. Environmental factors like humidity should be controlled as they can slightly alter the measurement of the air filled test cell.

The measurement of dielectric properties by wave propagation looks at phase shift, attenuation and/or reflection of electromagnetic waves as they move through a sample either in free space or within a section of transmission line. This technique relies on the relation between the complex dielectric constant and the wave propagation constant:

$$\gamma = \alpha + j\beta = \gamma_0 \sqrt{\varepsilon^*} = j\frac{2\pi}{\lambda_0 \sqrt{\varepsilon' - j\varepsilon''}} \tag{19}$$

where α is the attenuation constant, β is the phase constant, γ_0 is the free space propagation constant, and ε^* is the complex dielectric constant. Transmission (T) and

reflection (Γ) measures, typically done with the use of a network analyzer, can be related back to ε^* by:

$$T = e^{-\gamma} \tag{20}$$

and

$$\Gamma = \frac{1-\sqrt{\varepsilon^*}}{1+\sqrt{\varepsilon^*}} \tag{21}$$

Care must be taken to consider all possible boundaries and reflections within the test system. Once a signal graph is determined, ε^* can be calculated from T and Γ (Pozar, 1990).

Numerous patents and reviews indicate the function and effectiveness of various designs (Funk, 2001; Greer, 2002; Nelson, 2006; Lawrence and Nelson, 2000). Nelson notes that nearly all commercially available sensors utilizing the RF dielectric/impedance method use frequencies in the range of 1-20MHz (Nelson et al., 2000). More recent technological developments have enabled the cost effective production of VHF and microwave frequency sensors.

Research agrees that correction for the confounding factors of density and temperature must be accounted for in the design and operation of instrumentation. Equally important, research has shown that care must be taken in selection and fitting of calibrations to correlate moisture and instrument signals.

Material Classification Studies

Objectives

The examined instrument measures complex permittivity in grains and is designed to distinguish moisture content and density differences. The objective of this study is to evaluate potential uses for the instrument in granular materials. This goal includes verifying moisture and density measurement abilities, distinguishing between different materials, and classification by chemical composition.

Several experiments were conducted to determine instrument behavior. A series of experiments were conducted to evaluate the basic operation and behavior of the sensor. A second set of experiments were conducted to estimate material properties and their relationship to the sensor. A final experiment was conducted to assess the confounding physical properties of moisture, density, and temperature acting on the instrument.

Materials and Methods

Materials Tested

The major categories of materials evaluated included: ground and powdered feed ingredients, whole grains, soils, and granular fertilizer. In these trials, moistures were not controlled. Materials were allowed to equilibrate to ambient conditions (temperature and humidity), which were then held constant for that group of materials.

Apparatus

The instrument utilized in these experiments is a shunt mode capacitive measurement device (Greer, 2002). The sensor utilizes a microprocessor to control two direct digital synthesis chips. The microprocessor initiates a sinusoidal signal to a transmitting electrode in the sensor measurement chamber. At the receiver electrode, a

virtual ground amplifier biases and references the admitted signal. An analog multiplier synchronously demodulates the received signal with a second sinusoid. The second sinusoid alternates between in-phase and 90° out-of-phase, which allows the filtered demodulated signal to represent either capacitance or dielectric loss. Figure 5 shows a schematic representation of this function.

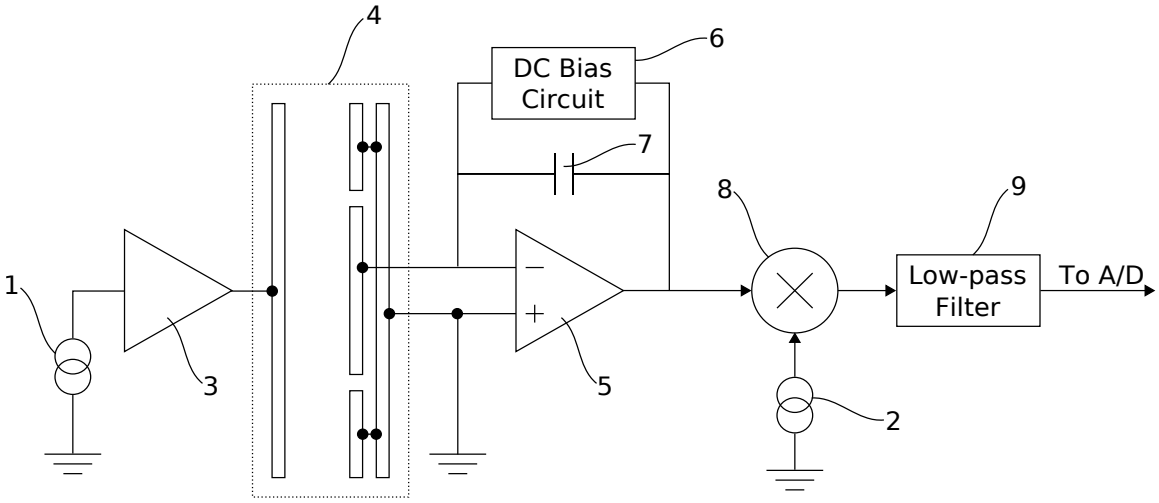

Figure 5: Schematic representation of commercially available sensor's analog circuitry. References in this figure: 1, 2: Microprocessor controlled direct digital synthesis oscillators; 3: Transmitter buffer amplifier; 4: Sensing chamber; 5, 6, 7: Receiver amplifier, bias and reference; 8: Analog multiplier; 9: Filter (Greer, 2002).

One configuration of this instrument, shown in Figure 6, utilizes a parallel plate capacitance chamber allowing grains to flow through the sampling cell. This sensing chamber will be hereafter referred to by its manufacturer part number: FT. The FT permits grain to flow through for continuous monitoring. For the purposes of laboratory evaluation of the instrument, a slide gate interrupts material flow, allowing the sensor chamber to fill with a static sample. The FT sensor chamber measures 12.70 cm (5.00 in.) wide by 17.78 cm (7.00 in.) tall, with a 5.08 cm (2.00 in.) space between excitation and sensing electrodes (Figure 6). The electrode plates are copper clad FR-4 printed

circuit board with 1.016 mm (0.040 in.) ceramic plating, measuring 12.70 cm (5.00 in.) wide by 15.24 cm (6.00 in.) tall. The design of the parallel plate chamber uses the entire transmit plate for a transmit electrode. The sensor uses a 6.35 (2.50 in.) by 8.89 cm (3.50 in.) portion of the receive plate for the receive electrode, with the remainder functioning as a virtual ground.

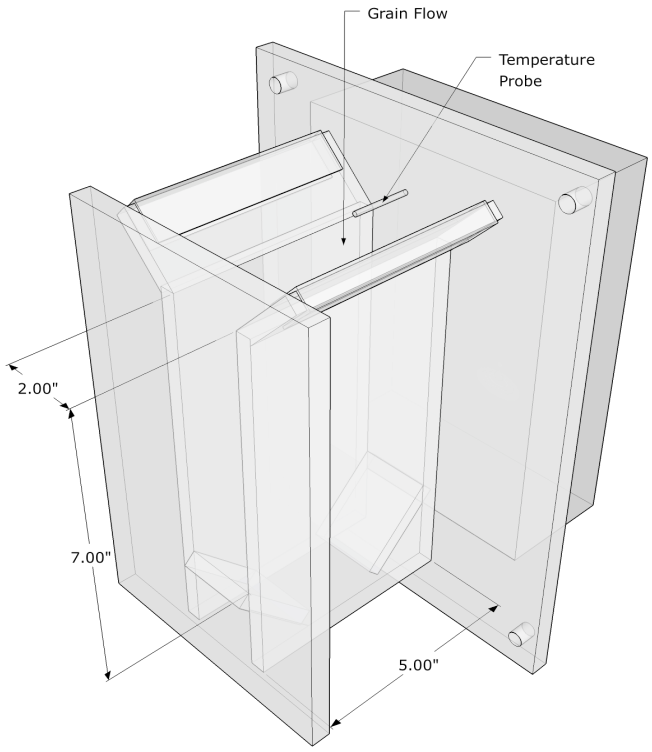

Figure 6: FT Sensor Cell Dimensions.

An alternate sensor chamber, part number FP utilizes a flat plate configuration. This alternate electrode configuration implements excitation and sensing electrodes on a copper clad FR-4 printed circuit board with 1.016 mm (0.040 in.) ceramic plating. However, this design places the electrodes side by side, separated by an electrode tied to the device's ground. The total size of the FP sensor is 12.70 cm (5.00 in.) wide by

17.78 cm (7.00 in.) long. An illustration of the FP electrode configuration is shown in Figure 7.

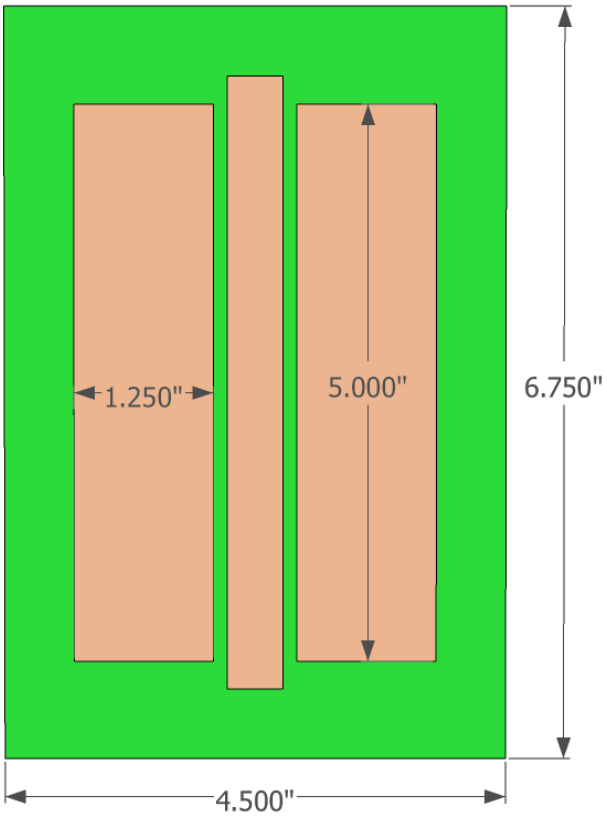

Figure 7: FP Sensor Surface Dimensions and Electrode Configuration.

The sensing instrumentation records capacitance and dielectric loss data for frequencies ranging from 3.125kHz to 6.4MHz by octaves. The instrument also records temperature from probes in the sample cell and on the circuit board. The sensor stores this data in a user interface that also provides calibration function (Rabbit Semiconductor OP7100). An RS-232 link between the user interface and a personal computer running a custom LabView software instrument allows logging of the sensor data (Labview, 1996). Figure 8 illustrates the devices used to generate and record capacitance and dielectric loss data.

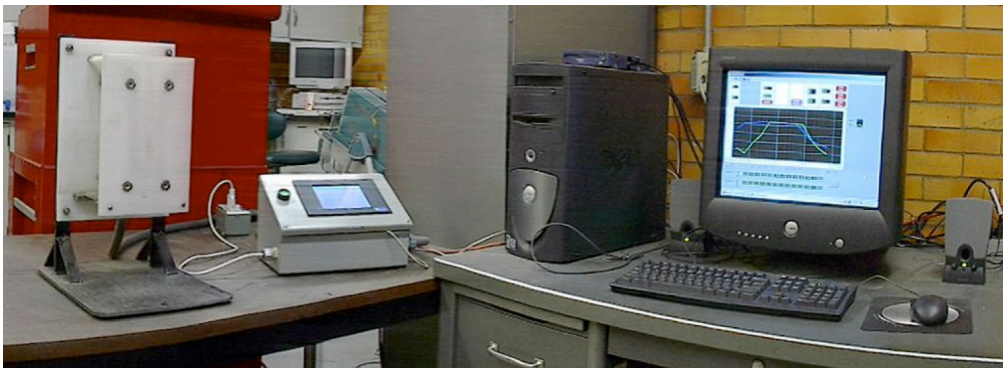

Figure 8: Sensor instrumentation, including FT sample cell and user interface connected to PC running LabView Software.

Observations

Linearity and Known Materials

In order to better understand sensor behavior and assure linearity, tests using some frequency constant dielectrics were conducted. If a material of known dielectric strength could be examined, then a true dielectric value could be assigned to any material examined in the instrument thereafter. In the context of examining physical effects on the sensor, the FP sensor cell was also examined to provide information about how depth of material affected the sensor's reading and to put the FP sensor readings in context with that of the FT sensor.

Materials

Fertilizer was examined to determine if a measure of the granular size distribution could be accurately and repeatably performed to predict granule size degradation. With fertilizer, granular size is an essential piece of information for proper application. The expectation was that as the fertilizer was broken down into smaller pieces, the amount of air between granules would decrease and would increase the signal to the instrument.

Using the sensor, it was predicted that a correlation could be made between the signal and the fertilizer's physical state.

Soils were examined with the instrument to find whether a relationship existed between soil type and the signal from the instrument. It was expected that each soil type could be linked to a response from the sensor, but density and moisture were anticipated to have a confounding affect.

Feed ingredients and whole grains were examined to determine if differences between ingredients existed. The expectation in this case was that each ingredient and whole grain would have independent dielectric characteristics based on moisture and physical shape and size, but also on the chemical makeup of the tested sample. These differences in the multi-frequency spectra would reveal a way to distinguish one material from another. It was expected that each material could be associated with a certain sensor response and that moisture and density could be correlated to the instrument's response. The ultimate goal would be using the instrument as a one-size-fits-all moisture and density monitor and/or as a sentry in a grain processing facility.

Data and Analysis

Constant Dielectrics

As a starting point for experimentation for the multi-frequency, capacitive sensor and FT sensor, samples with dielectrics which had limited frequency dependence were examined. The FT sensing cell was lined with a plastic Ziploc bag to accommodate liquid (corn oil) for this experiment. The plastic lining caused a very slight deviation in

comparison to air alone, but the effect was within the limits of the variation of the sensor itself, and hence ignored. These results are shown in Figure 9.

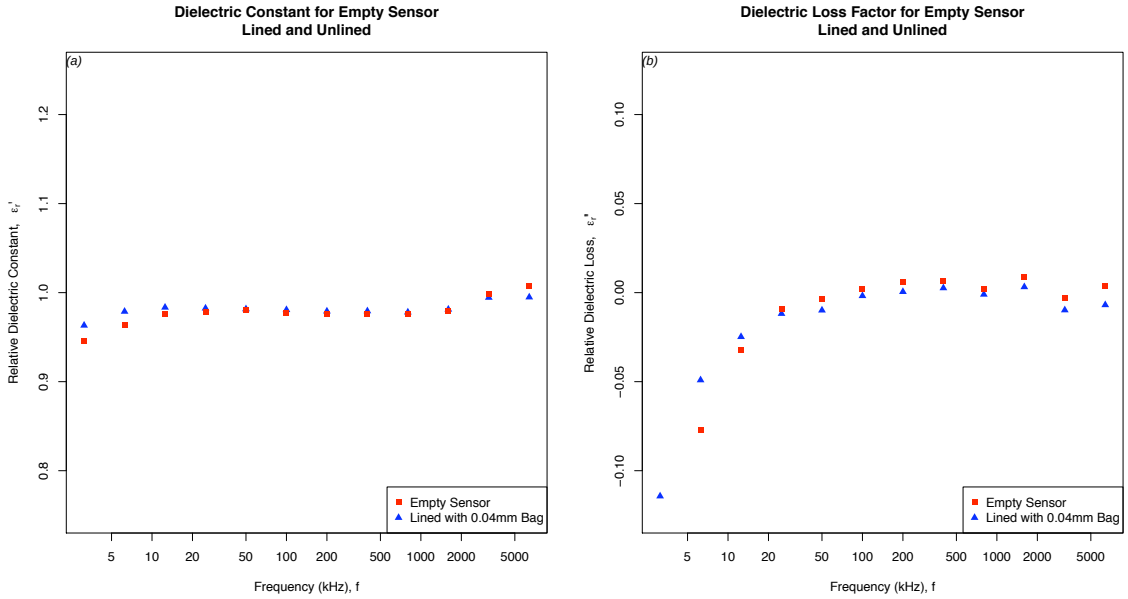

Figure 9: Variations in open air due to plastic liner (a) of dielectric constant and (b) loss factor.

A mixture of 2, 3, and 5 mm glass beads was added to the FT sensor's lined cavity. Readings from the sensor were taken once just as the beads were added, then again while the cavity was shaken to eliminate any bridging and poor packing of the glass. The cavity was shaken until no further change in signal was observed. Similarly, once the signal from the glass had stabilized, corn oil was added to the FT sensor's cavity. Again, readings were taken at intervals until the signal from the instrument no longer varied between measurements.

The signal from glass beads that filled the cavity to approximately 50% volume (the rest of the volume being occupied by air), was slightly over half of that expected from solid glass. When corn oil was added, increasing the volume occupied by the

dielectric to 100%, the observed capacitance reached an expected value for the mixture of corn oil and glass. The measured response by the FT sensor is shown in Figure 10. The instrument gave a reasonably flat response across all frequencies, as it should have for the materials examined. Also, as expected, the measured loss factor was near zero for these materials.

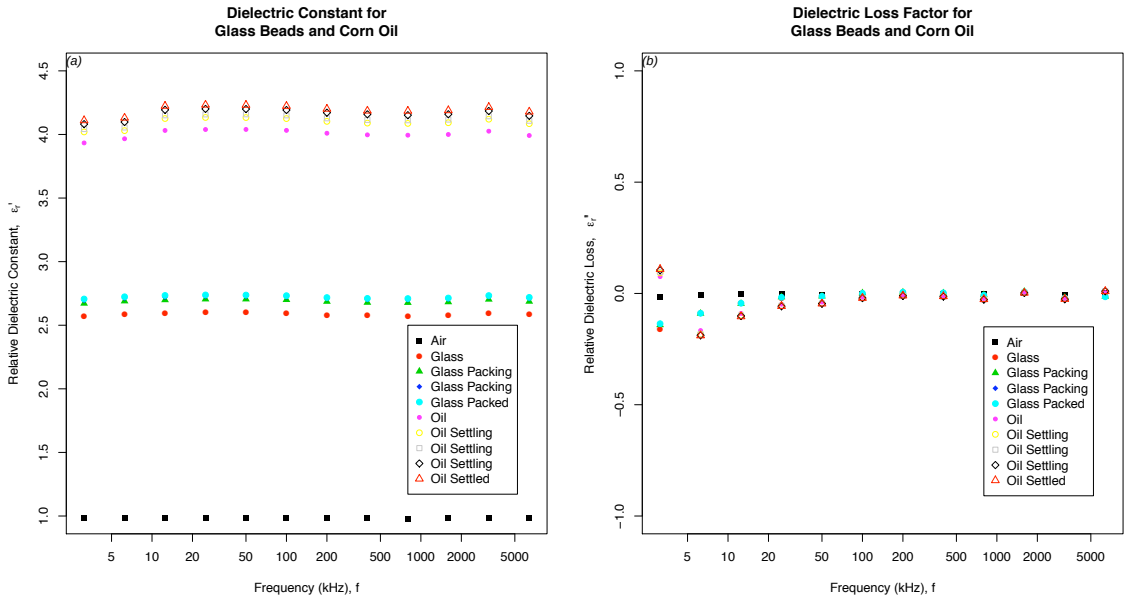

Figure 10: Linear dielectrics evaluated with packing density variations observed (a) for dielectric constant and (b) loss factor of glass beads in corn oil.

Flat Plate Depth

The FT sensor cell's configuration was a well-known physical arrangement. If the material to be examined was between its two parallel plates, the instrument would collect and display the relevant data. Fringe fields are minimized by the FT sensor's configuration. However, for the FP sensor configuration, fringe fields become relevant. Further, with no defined sample cell (as in the case of the FT) the sample depth can be varied. A simple experiment was designed to discover how different depths of sample affected the data collected by the instrument.

The FP sensor was laid at the bottom of a tub and corn was placed in the tub above the sensor at varying levels. In the following graphs, both measured capacitance and loss were affected by the amount of grain present above the sensor face. As the depth of the corn increased, the value read by the sensor for either capacitance or loss asymptotically approached a value.

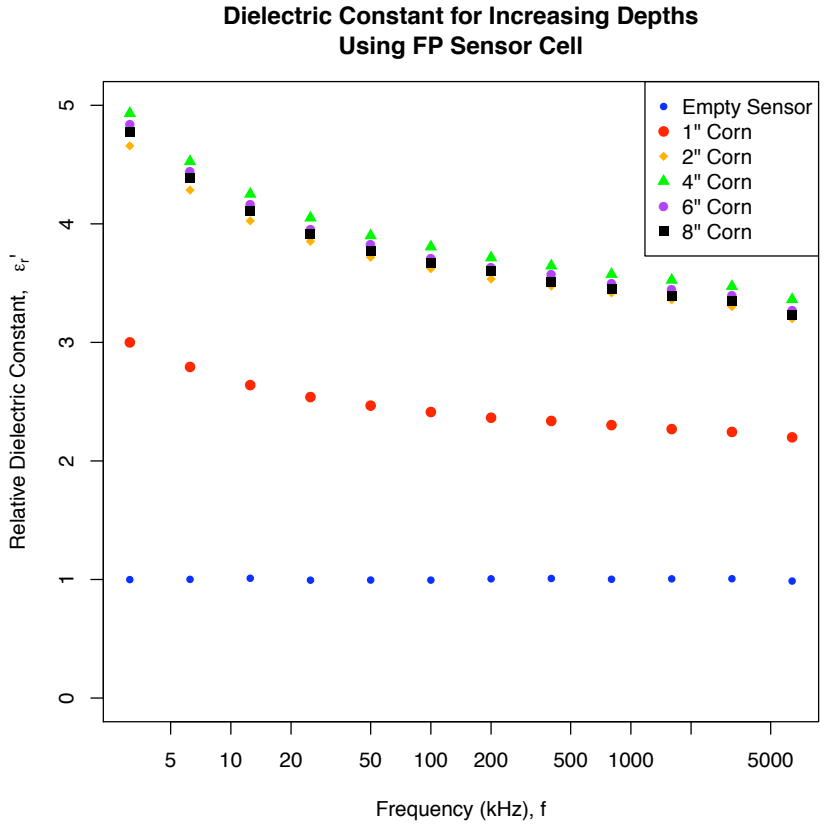

Figure 11: Depth effect on measure of dielectric constant with FP sensor cell.

It should be noted that the 15 and 20 cm (6 and 8 in.) samples did not continue this trend, but instead decreased the reading of the instrument. Further experimentation showed that this decrease was likely due to variations in the physical arrangement of the kernels. (See notes on static versus flowing samples for another example.) Hence,

beyond the 10 cm (4 in.) range for typical samples of corn, the instrument was able to observe no differences.

Static versus Flowing Samples

Would static samples adequately approximate the dynamic samples seen in the application of the FT sensor cell? If static samples could not be used, material would have to be allowed to flow through the sensor, making sampling in the laboratory much more difficult. This question was answered empirically.

Soybeans were obtained from the University of Minnesota's agronomy department. Enough seeds of a particular lot were collected to allow them to flow through the FT sensor cell with partial restriction while data from the instrument was collected. Figure 12(a) shows an example of the flowing samples, compared to a typical static sample of the same soybean lot.

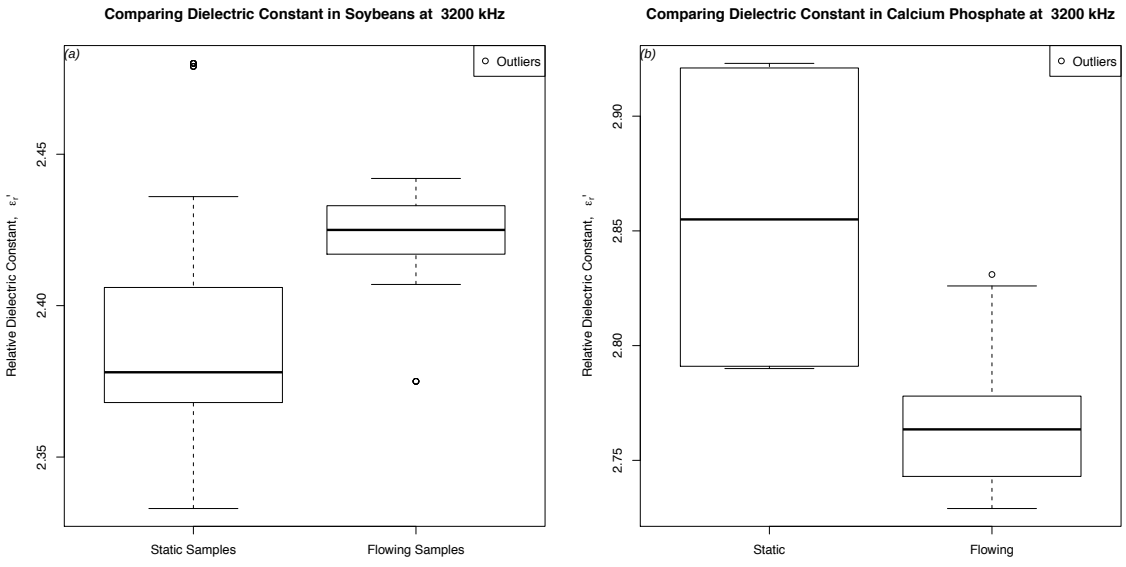

Figure 12: Boxplot of pooled static sample measurement of relative dielectric constant compared to flowing sampling for (a) soybeans and (b) calcium phosphate at 3200kHz.

The sensor repeated itself across all frequencies, showing that the flowing samples fell within the bounds of the multiple static samples; in this case fifteen samples were pooled to give a range for static sampling. The measured result of flowing soybeans was slightly higher than the identical material measured at rest. A similar experiment was done with calcium phosphate obtained from a local feed manufacturer. In this case, flowing sampling resulted in a slightly lower measurement, shown in Figure 12(b). This result may suggest that there is some bias from either bulk density or material geometry that causes the calcium phosphate to measure lower when sampled while flowing and the soybeans to measure higher. However, any bias is small compared to the sampling error.

An adequate method is therefore to approximate the flowing material sampling by filling and emptying the sensor several times for each material. This avoids the logistical problems of handling greater volumes of material. Collecting multiple data points allows for approximation of the true mean better than single static samples.

Fertilizer

The question was raised as to whether the instrument could be used to determine fertilizer degradation. Theory behind capacitive sensing at kilohertz to low megahertz frequencies dictates that water has the primary influence on dielectric strength, and with density having a secondary affect. Since degraded fertilizer would be in smaller pieces, the packing density will therefore increase and a noticeable increase in signal from the FT sensor should be seen.

To test this hypothesis, a commercially available fertilizer was purchased. A single grain size analysis of the un-degraded fertilizer was done and the results are shown

in Figure 13. The results of the sizing were consistent with standards for analyses of other common granular materials (ASABE, 2008a).

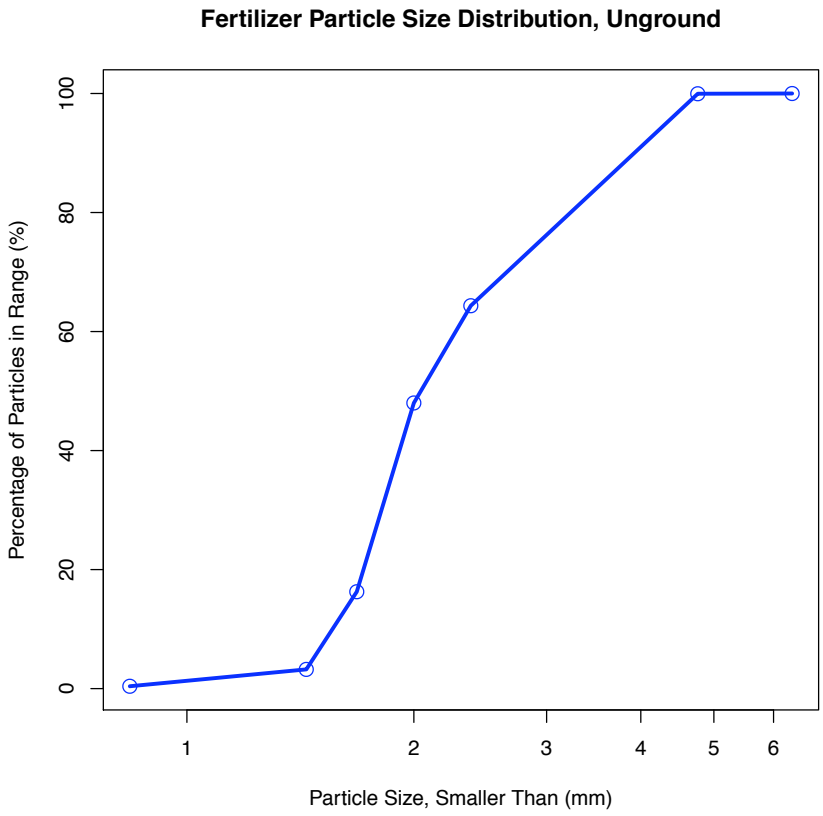

Figure 13: Initial fertilizer granule size distribution over six sieves.

Three lots were created from the remaining material. Sample one was examined with the sensor as it was, straight from the bag. A small roller mill was then used to degrade samples two and three. Sample two was ground for one minute and sample three for two minutes in the mill. In both cases, the roller mill degraded the fertilizer evenly, without grinding all granules to a fine powder.

As can be seen in Figure 14, the performance of the instrument was more than adequate to show a correlation between degradation of the fertilizer and the capacitive and loss signals received at and above 200kHz. (Signals below this frequency exceeded

the instrument's range and are therefore irrelevant, as evidenced by the plateau across the 5-150kHz range.) More study would be necessary to quantify the relationship and remove the moisture dependence variable.

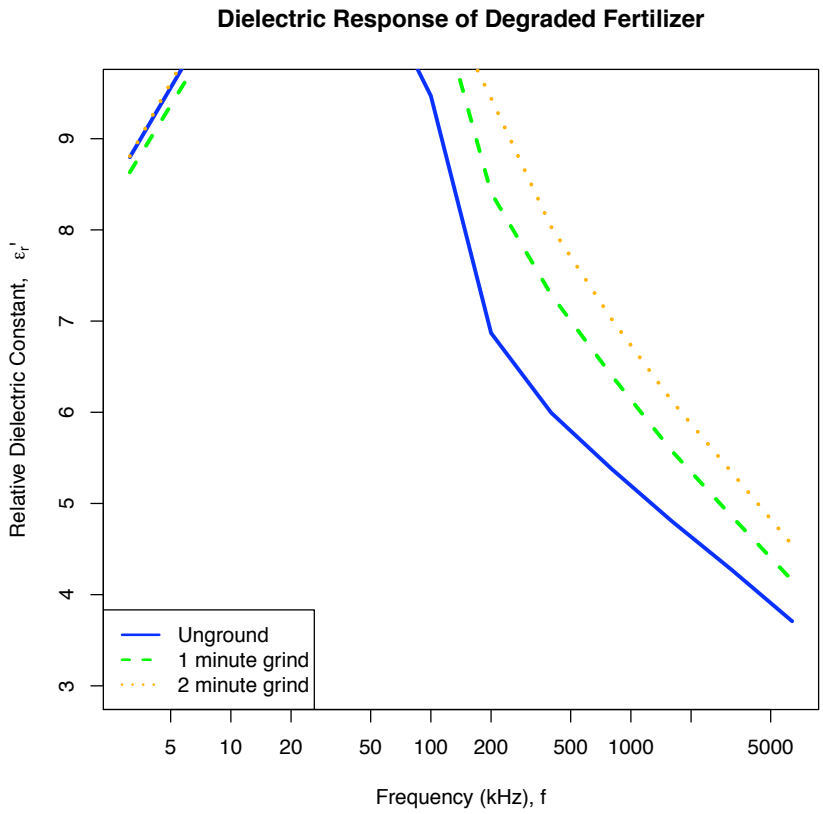

Figure 14: Response of dielectric constant in ground fertilizer.

Soil

Along the same vein as the investigation into fertilizer degradation came the idea that soil types could be identified by the tested instrument. A desired instrument would be able to detect a five percent change in soil compositions. The various types of soils seen throughout the region vary by their component size distribution. The major component groups are sand, silt, and clay. Different combinations of these ingredients

were mixed with each other as well as with existing soils to show whether or not differences could be seen between slightly dissimilar soils.

Table 1 shows a brief summary of the relative dielectric data for representative soil components at 3200kHz. There is a wide range of variation between the different ingredients (dielectric constants from 2.23 to off-scale). A complete graph of the entire frequency range is shown in Figure 15. The soils' dielectric constant decreases over increasing instrument frequency. Note that several of the materials exceed the range of the sensor between 5 and 100kHz. It is also noteworthy that the complex soils read lower than any constituent ingredient. In samples examined, moisture was not controlled, however all samples were equilibrated to the sampling environment prior to testing.

Table 1: Summary of basic soil materials and their dielectric constant at a frequency of 3200kHz.

Material	ε'
Clay	5.95
Silt	6.24
Dried Silt	3.05
Damp Silt	Off-Scale
Sand (#2)	4.71
Sand (#7)	7.39
Silty Loam Soil (Hubbard)	2.82
Silty Loam Soil (Other)	2.23

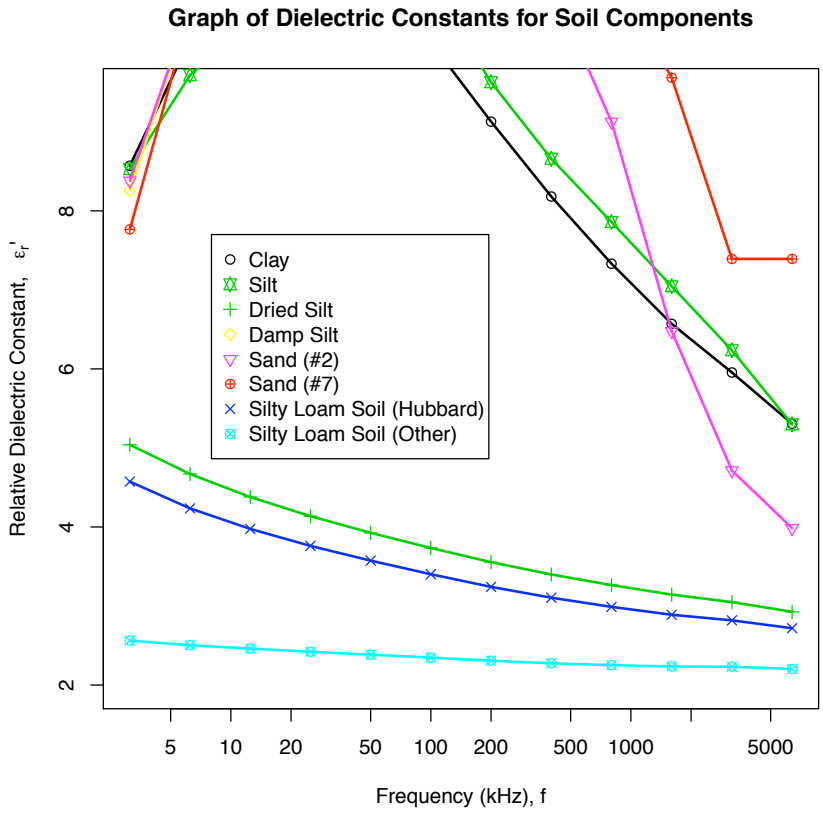

Figure 15: Dielectric of common soil components and their dielectric constants.

A single mixture of sand was added to the silty loam soil (Hubbard) and additional sand measurements were taken with the silty loam soil (Other) at rates of 5, 10, 20 and 40% (by volume). For the silty loam and sand mixes, the pure sand samples had much larger measured capacitances than the combined samples. Depending on the size of sand grains added to the silty loam, the signal changed accordingly. In the Hubbard soil, the addition of sand caused a decrease across all frequencies. Figure 16 shows this relationship.

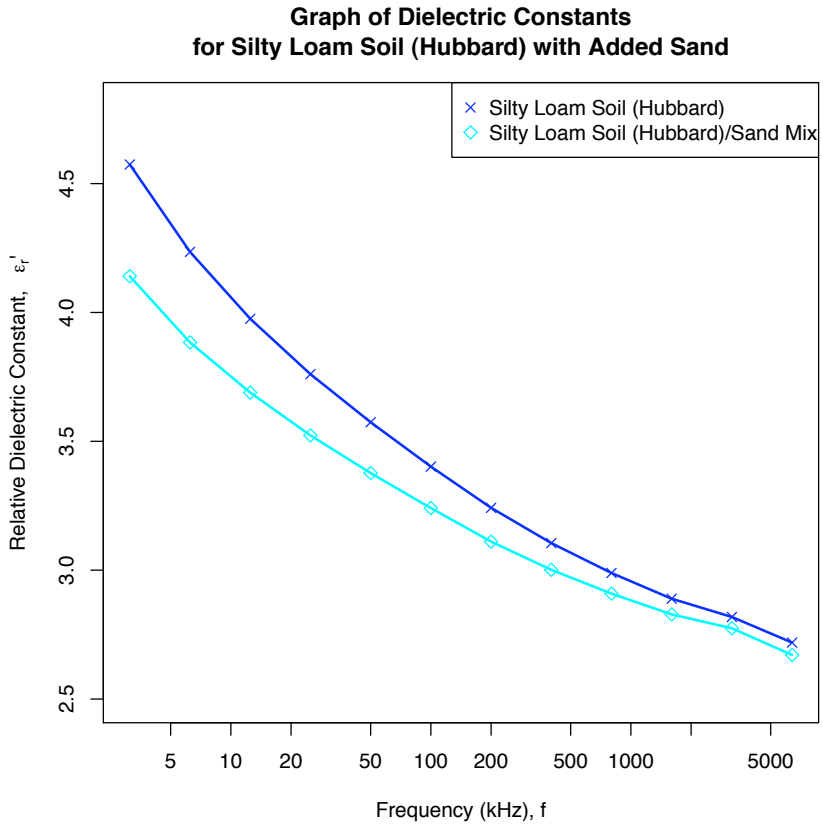

Figure 16: Dielectric constant measured for silty loam soil (Hubbard) with added sand.

When sand was added to the silty loam soil (other) it generally increased the signal. The most drastic change was seen with the coarse sand (#2, 0.5-1.0 mm), which shifted the capacitance up across all frequencies as shown in Figure 17(b). The fine grain sands had other effects on the capacitance. For the fine (#7, 125-250 μm) sand, the capacitive values increased with the addition of the sand (Figure 17(c)). However, as more was added, the lower frequencies saw a decrease in signal (to a point lower than the original silty loam), and the upper frequencies stayed approximately the same.

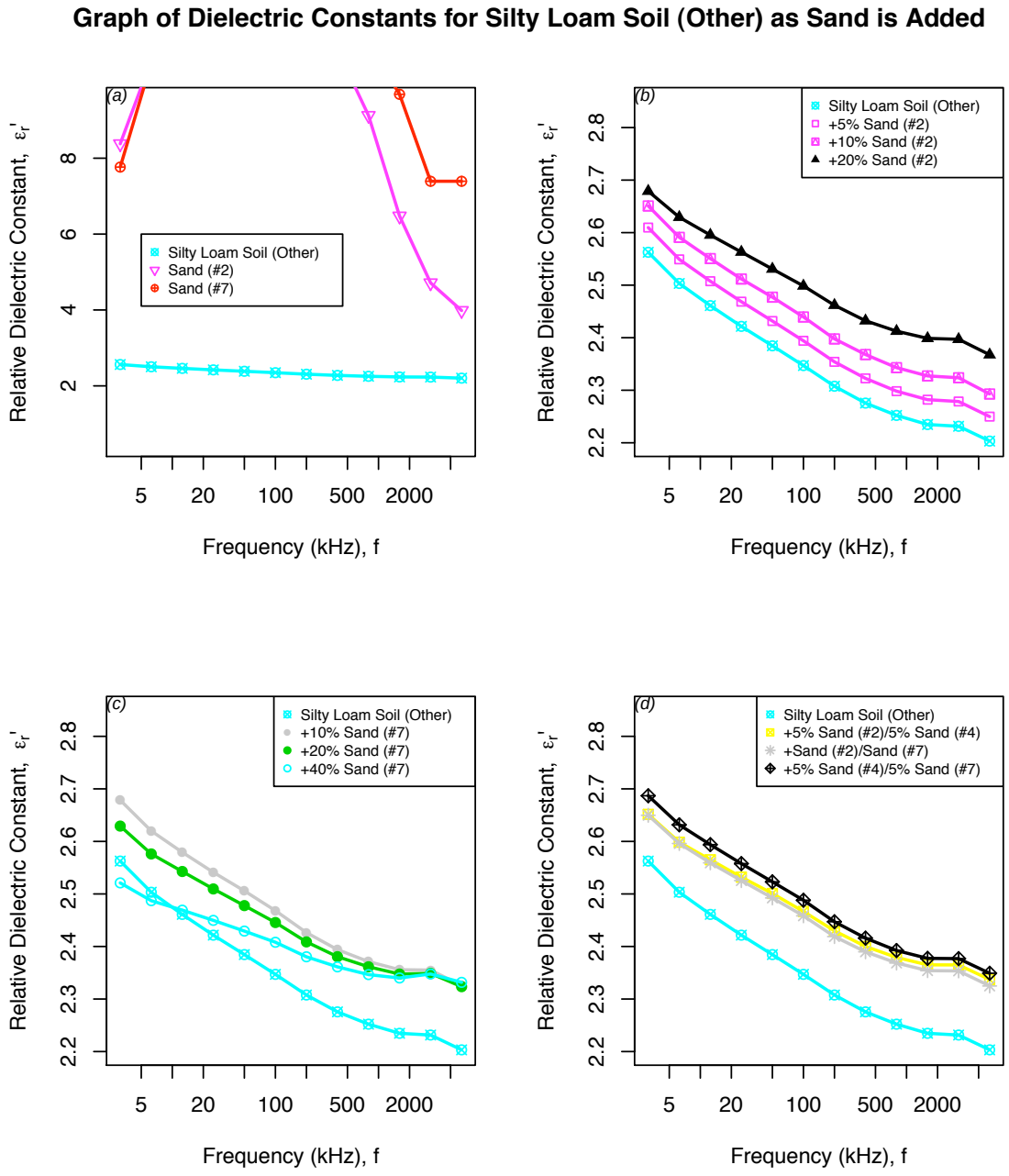

Figure 17: Dielectrics constants for silty loam soil (other) when mixed with varying fractions of sand.

Considering the original problem statement, can the instrument be used to detect differences in soils at a five percent level? For certain elements in certain soils the sensor does well. The best example is the addition of coarse sand to silty loam soil, where a five

percent addition was significant across all frequencies. Unfortunately, soils in practice will have varying moisture contents. The problem then becomes having a sensor that can measure larger capacitances and not be confounded by the variation in moisture contents. Caveats aside, the experimental data showed promise that the instrument could be calibrated to measure changes in soil composition.

Feed Stuffs and Grains

A variety of ground meals and other feed ingredients were obtained to create a reference spectra. The list of feed ingredients is shown in Table 2. Figure 18 depicts the capacitive spectra observed by the instrument for each sample. It can be noted that the granular compounds (salt and calcium carbonate) had a very flat response over the range of frequencies and independent of dielectric constant. Linearity of response was judged by residual variation on a linear regression. Non-linear models had a variation in residuals of at least 10% of the relative dielectric and a noted "U" shaped residual response over frequency.

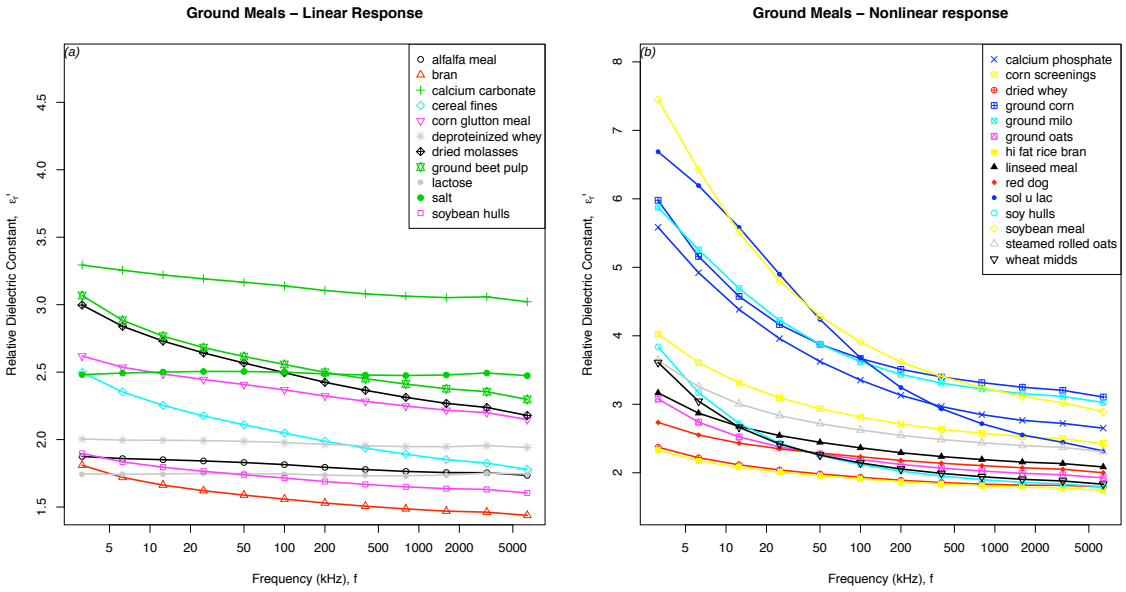

Figure 18: Feed ingredients' dielectric constant response for (a) linear and (b) nonlinear materials.

The instrument was equipped to obtain moisture and density values from corn. It was reasoned then, that there may be additional data readily obtained from the sensor, which corresponded to other physical parameters, including kernel shape, size, and even nutritional value. Therefore, data from numerous varieties of several different grains was collected. The four major components of this experiment included corn, soybeans, wheat, and as previously discussed, ground meals and feed ingredients.

Table 2: Feed ingredients with response at 3.125kHz and 200kHz.

Product	Response	ε' @ 200kHz	ε' @ 3.125kHz
Alfalfa Meal	Linear	1.79	1.87
Bran	Linear	1.53	1.81
Calcium Carbonate	Linear	3.11	3.29
Calcium Phosphate	Nonlinear	3.13	5.58
Cereal Fines	Linear	1.99	2.50
Corn Glutton Meal	Linear	2.32	2.62
Corn Screenings	Nonlinear	2.71	4.03
Deproteinized Whey	Linear	1.96	2.00
Dried Molasses	Linear	2.42	3.00
Dried Whey	Nonlinear	1.89	2.37
Ground Beet Pulp	Linear	2.50	3.07
Ground Corn	Nonlinear	3.51	5.98
Ground Milo	Nonlinear	3.44	5.87
Ground Oats	Nonlinear	2.12	3.08
Hi Fat Rice Bran	Nonlinear	1.87	2.33
Lactose	Linear	1.74	1.75
Linseed Meal	Nonlinear	2.29	3.17
Red Dog	Nonlinear	2.18	2.74
Salt	Linear	2.49	2.48
Sol U Lac	Nonlinear	3.24	6.69
Soy Hulls	Nonlinear	2.02	3.84
Soybean Hulls	Linear	1.69	1.90
Soybean Meal	Nonlinear	3.62	7.45
Steamed Rolled Oats	Nonlinear	2.55	3.64
Wheat Midds	Nonlinear	2.06	3.61

Figure 19 and Figure 20 illustrate each crop seed's response by variety. For corn, two varieties of hybrid seed were examined. One was a waxy corn with high oil content, hybrid number N4342Wx from Syngenta Seeds. The other was a Bt variety, N4242Bt, also from Syngenta. One lot of each grain was tested after being allowed to equilibrate to ambient conditions. Each lot was sampled 10 times with 12 replicates. One standard deviation from the average sample collected is shown as an error bar on each data point. The two corn hybrids showed significant differences in their capacitive spectra as observed by FT sensor cell.

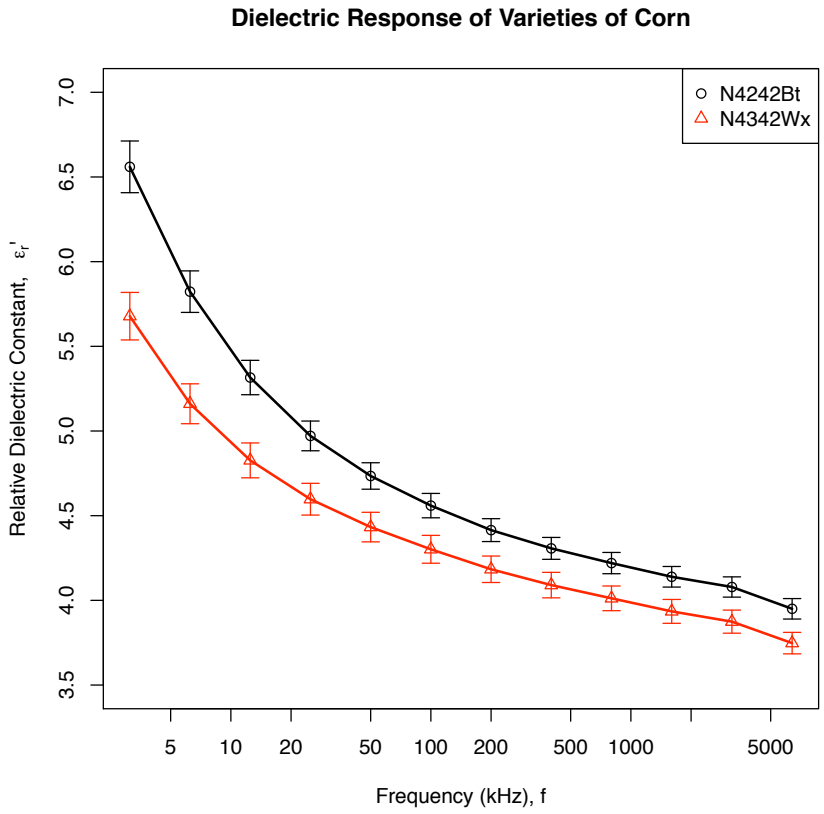

Figure 19: Dielectric response of varieties of corn.

24 varieties of wheat were examined with the instrument. All varieties of wheat were obtained from the University of Minnesota Agronomy Department. As can be seen from Figure 20(a), the variation between varieties was so small, variation within samples made it difficult to differentiate the individual wheat samples using the capacitive spectra.

A number of soybean varieties were also made available by the University of Minnesota Agronomy Department. 15 different varieties of internally bred and commercially available soybean seed were tested. The capacitive spectrum of the soybeans was somewhat wider than that of wheat, but still too close for inter-varietal differentiation. Figure 20(b) does illustrate that a few varieties stood out due to large or

small seed size. IA2050 and M97-206017 had seed sizes of approximately 25% less and 50% greater than the mean seed diameter of other varieties respectively. However, most varieties filled in the space between.

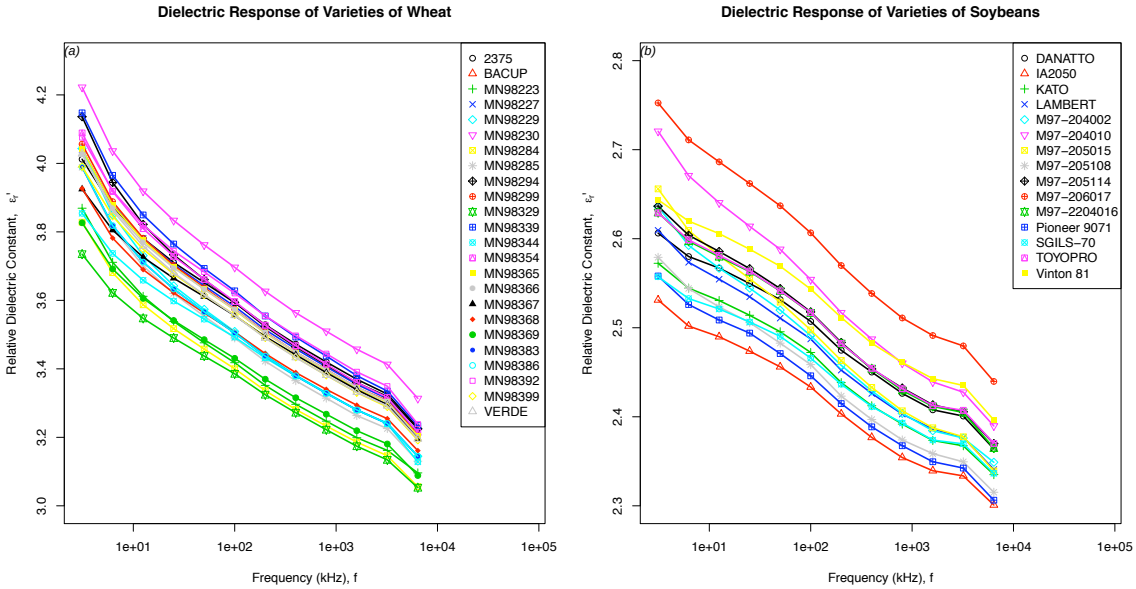

Figure 20: (a) Wheat and (b) Soybean dielectric response among multiple varieties.

Pattern Recognition

No clear path to inter-varietal identification of wheat and soy was found due to the statistical insignificance of variations between varieties. Since inter-varietal identifications could no be made, it was proposed that the sensor be used as a classifier to make inter-material-type identifications. Again, the four major categories of classification were deemed to be the seeds of corn, wheat, soybeans, and the general category of feed ingredients and other ground meals.

Pattern recognition algorithms were determined to be an efficient way of programming the sensor to be a classifier. The first step in using pattern recognition is to determine what data is significant. Since the capacitances at all twelve frequencies of the

instrument were assumed to be meaningful, the most logical way to reduce the data set was to create fourth order polynomials, which were frequency dependent. This set of polynomials collapsed the twelve frequency points into five coefficients for each sample.

Using a technique called Fisher's criterion to create maximum separation between points, several possible correlations of the samples to a two-dimensional coordinate system were reached as shown in Figure 21 (Webb, 2002; Braun, 2003). The final step in implementing pattern recognition was to determine a method to classify the points based on where each point was in relation to one another. A commonly used classification method is k-nearest neighbors.

Implementation of this pattern recognition scheme brought forth error rates of below five percent on initial training sets. However, because concerns about the confounding effects of moisture content were not closely examined in this experiment, further data was not collected for this classifier. Instead an experiment to investigate moisture dependence of the instrument was carried out.

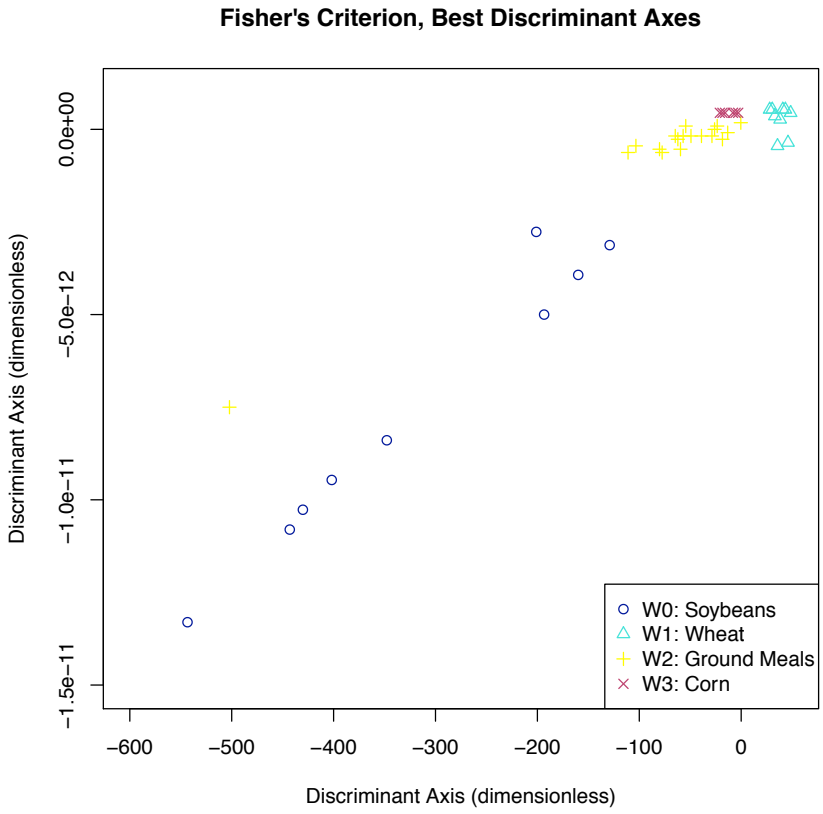

Figure 21: Best discrimination axes using Fisher's criterion.

Moisture Dependence

The cumulative experiment in this segment of study was to look at several different types of crop seeds and the effect moisture variation had on the instrument. The objective was to use the data as a training algorithm for a classifier using pattern recognition.

The experiment was set up as a randomized block. Moisture was controlled for, but density was not. Three replicates of each of six moisture levels for each of the three different seeds (corn, wheat and soy) were prepared. Samples needing to have moisture added were re-wet using the standard procedure of adding distilled water, tumbling the wetted grain for two hours and then placing it a sealed container just above 0°C for 72

hours. This allowed moisture to be fully absorbed into the seed and minimize any unbound water or moisture gradients. Prior to sampling, the sealed bags of grain were removed from the cooler and allowed to equilibrate to room temperature (22.5°C).

Samples were not large enough to accommodate sampling moving grain, so simple static samples were taken. Through the instrument's data acquisition, 10 samples of each replicate were obtained. Once data had been gathered from the FT sensor cell, samples were re-bagged to allow for oven moisture measurements. ASABE standard S352.2 methods were used to obtain moistures for each of the 51 samples listed in Table 3 (ASABE, 2008b).

Table 3: Moisture values for corn, soy, and wheat.

Sample #	Variety	Sample M.C.	Sample #	Variety	Sample M.C.
37	Corn: N43-C4	13.7	13	Soy: IA2050	17.6
51	Corn: 44-46	13.5	31	Soy: SGILS-70	17.7
48	Corn: N43-C4	13.7	21	Soy: ToyoPro	19
17	Corn: N43-C4	16.7	24	Soy: M97-204010	19.8
49	Corn: 44-46	16.6	53	Soy: Vinton 81	19.6
52	Corn: 44-46	16.3	15	Soy: M97-205108	22.8
44	Corn: N43-C4	18.3	19	Soy: M97-206017	24.1
5	Corn: 44-46	20.5	4	Soy: Pioneer 9071	21.8
35	Corn: 44-46	20	9	Wheat: MN98365	15.3
30	Corn: N43-C4	22.2	41	Wheat: MN98223	19.7
12	Corn: N43-C4	21.5	32	Wheat: MN98339	14.9
38	Corn: 44-46	21.7	11	Wheat: MN98294	19.7
26	Corn: N43-C4	22.4	43	Wheat: MN98366	17.7
6	Corn: 44-46	24.1	27	Wheat: MN98331	20.7
29	Corn: 44-46	23.9	8	Wheat: MN98392	19.6
40	Corn: N43-C4	26.4	47	Wheat: MN98221	23.1
14	Corn: N43-C4	26	39	Wheat: MN98230	22.2
1	Corn: 44-46	25.1	22	Wheat: MN98368	24
54	Soy: M97-205015	11.3	50	Wheat: MN98367	22.7
20	Soy: M97-204002	11	45	Wheat: MN98354	23
18	Soy: Kato	11.4	2	Wheat: MN98229	27
25	Soy: M97-224016	14.4	3	Wheat: MN98334	27.5
23	Soy: Danato	15.2	28	Wheat: MN98299	28.8
10	Soy: Lambert	14.1	34	Wheat: MN98287	28.1
			33	Wheat: Verde	29.7

When all of the data was collected, it was found that the data set was too small to run a pattern recognition algorithm. From the data set, it was determined that the differences between grains were not great enough to overcome the dominant relationships between capacitive spectra and physical properties of moisture and density.

An analysis of the dependence of moisture on capacitive output from the instrument follows in Table 4. Each of the capacitive values at frequencies 5 (50kHz), 8 (400kHz), 10 (1600kHz), and 11 (3200kHz) made significant contributions to the relationship between moisture and capacitance (Oehlert and Bingham, 2000).

Table 4: Regression of parameters with contribution to moisture.

Regression of model: moisture = C05 + C08 + C10 + C11				
	Coef. Est.	Std. Err.	t	P-value
CONSTANT	-8.206	3.319	-2.472	1.719E-02
C05	0.921	0.223	4.127	1.529E-04
C08	10.028	1.575	6.368	8.124E-08
C10	-49.325	9.549	-5.166	5.030E-06
C11	44.059	9.045	4.871	1.353E-05
Anova of above model:				
	Deg. of Freedom	Sum of Squares	Mean Square	
CONSTANT	1	20916	20916	
C05	1	917.94	917.94	
C08	1	20.91	20.91	
C10	1	61.86	61.86	
C11	1	69.76	69.76	
ERROR	46	135.24	2.94	

Any attempt to make other relationships out of the data set obtained in this experiment resulted in poorly correlated functions. As a final result, the instrument did well at sensing moisture in whole grains, but poorly at sensing other physical parameters of the grain due to its strong primary dependence on water.

Conclusions

The assumption was made at the outset of this research that the commercially available sensor could measure moisture and density effectively and independently of the complex permittivity readings retrieved by the laboratory interface. However, this data was not independent, but instead closely tied to the ability of the instrument to read moisture and density. This incorrect assumption led to overlooking the acquisition of crucial moisture and density data for all but a few of the many observational studies. The effects of moisture and density confound the results of the remaining studies.

However, numerous qualitative results based on the behavior of the sensor supplied useful information. The instrument examined gave a linear response to linear

dielectrics with relative complex permittivities within an expected range. Differences between static samples and moving samples were compared in the FT sensor cell showing that static samples could be used to approximate a dynamic sample. The FP sensor cell configuration was evaluated and compared to the response from the FT sensor cell. It was found that the depth of product at the FP sensor cell needed as little as 10 cm (4 in.) for proper measurement.

Relationships between density and permittivity were found which could provide the basis for future study. The degradation of granular fertilizer showed a clear relationship between increasing permittivity and increasing density at constant moistures. Differences in some soils at constant moistures were also shown to have a monotonic relationship with permittivity. Variations due to moisture content in these materials were not investigated at this time.

Feed ingredients and whole grains were found to be surprisingly similar in their measured relative permittivities. The assumption was made that varietal differences within individual grains would either overwhelm the correlation with moisture, or that these differences would be insignificant. Through the use of pattern recognition techniques, a classifier was trained on data from numerous varieties with reasonable success at differentiating between grain types. However, moisture remained a confounding variable. A final attempt to remove the effect of moisture only underscored the strength of the relationship between moisture and measured permittivity. These results provided the basis for additional study with grains whose moisture and density could be well controlled.

Flowing Grain Studies

Objectives

Previous analysis of the commercially available instrument left questions about the validity of the algorithms implemented in calculating moisture and density from multiple measures of the dielectric constant and loss factor in grains and other materials. In 2005, the manufacturer developed a replacement for the original sensor, hereafter referred by its part number: A4MS. This revised device utilized the same FT and FP sensing chambers, but had additional capabilities that addressed some of the problems with the original instrument. The objective of studying this device was to evaluate existing density independent functions published in the literature and by the inventor, and to determine what level of accuracy while sensing both moisture and density in grain could be determined (Trabelsi et al., 1998; Funk et al., 2007; Greer, 2005).

This study was designed to remove the variables of hand filling the instrument and to look at bulk density variations. Additionally, the instrument allowed a much greater dynamic range to prevent the clipping of high dielectric values as occurred in initial studies. Multiple sensor sample cells were evaluated to test for differences in measurement by grain presentation and sensor configuration.

The calibration algorithms for the original instrument were based on a limited data set with most bulk density variations induced by packing density changes. The literature maintains that packing density is only part of the density variation measured by dielectric methods (Funk et al., 2007). Since packing density variations are difficult to control, in this study multiple varieties of #2 yellow dent field corn were obtained from a local grain producer's test plot yielding naturally induced changes in bulk density. To

control packing density fluctuations and avoid artificial bias, a continuous stream of grain was allowed to flow through the instrument's test cell rather than taking static samples. In the original instrument, many readings at mid-range frequencies for high-dielectric samples were off-scale. An internally adjustable gain control was implemented in the revised instrument. This control resulted in more usable data to evaluate over all frequencies.

In initial experimentation, the FP configuration was subjected to a basic evaluation. In this study, both FT and FP configurations were tested in tandem. This allowed comparison between the two configurations to evaluate any advantages or disadvantages inherent in either sample cell.

Numerous methods of correlating moisture to dielectric measurements have been cited by the literature. This study will evaluate both density dependent and density independent methods of instrument calibration to determine both the best accuracy and the most robust methods of predicting moisture and density. New relationships between density and moisture at kHz and low MHz relationships were sought to provide optimal calibration for the instrument.

Materials and Methods

Grains tested

Yellow #2 field corn was obtained from a local grower's variety test plot. This allowed for a sampling of 16 varieties of grain ranging in bulk density from 0.70 to 0.77 g/cm^3. Initial moisture contents of the corn ranged from 16.0% to 18.5% wet basis moisture. The corn was prepped for experimentation by removing excess chaff and fines

by air separation. The removal was done shaking the grain on 4.76 mm wire mesh grating with air blown across until most of the fines were removed. The corn was stored at room temperature and allowed to air-dry in 27 kg paper grain sacks, two sacks per grain type. During the experimentation, each bag was sampled and if moisture variation between bags of the same grain type was significant, the separate lots of the same grain were remixed and allowed to equilibrate.

Over the course of the experimentation the grain samples dried significantly. A protocol for re-wetting grain developed at the University of Minnesota's Department of Biosystems and Bioproducts Engineering was used to reconstitute the grain to desired sample moistures. Lots of grain were tumbled at approximately 4 RPM in a 60 L axially rotating drum (35.6 cm diameter x 66.0 cm length). Water was added two to three percent by weight at a time and the resulting mixture was tumbled for two hours. When the water was adsorbed, the grain was re-bagged, sealed and allowed to equilibrate for no less than 72 hours at 10°C. Due to the size limitation of the 60 L wetting drum, each half lot (13.5 kg) of grain was re-wetted individually rather than as a single sample. Several cycles through the sampling apparatus mixed the lots thoroughly and differences between the two lots of each sample were not observed.

Apparatus

In order to provide a continuous sample to the FP and FT sensor sample cells, a pneumatic conveyor was constructed from 10 cm (4 in.) PVC piping. The grain was conveyed using a blower fan (Hartzell Corporation Series 07) producing approximately 14.2 cubic meters per minute of airflow. A 19 L (5 gal) loading hopper filled this system and allowed for approximately 6.8 kg of corn per minute to be continuously cycled

through the sensor test cells and returned to a buffer hopper above the sample cells where it could gravity feed into the sensors below.

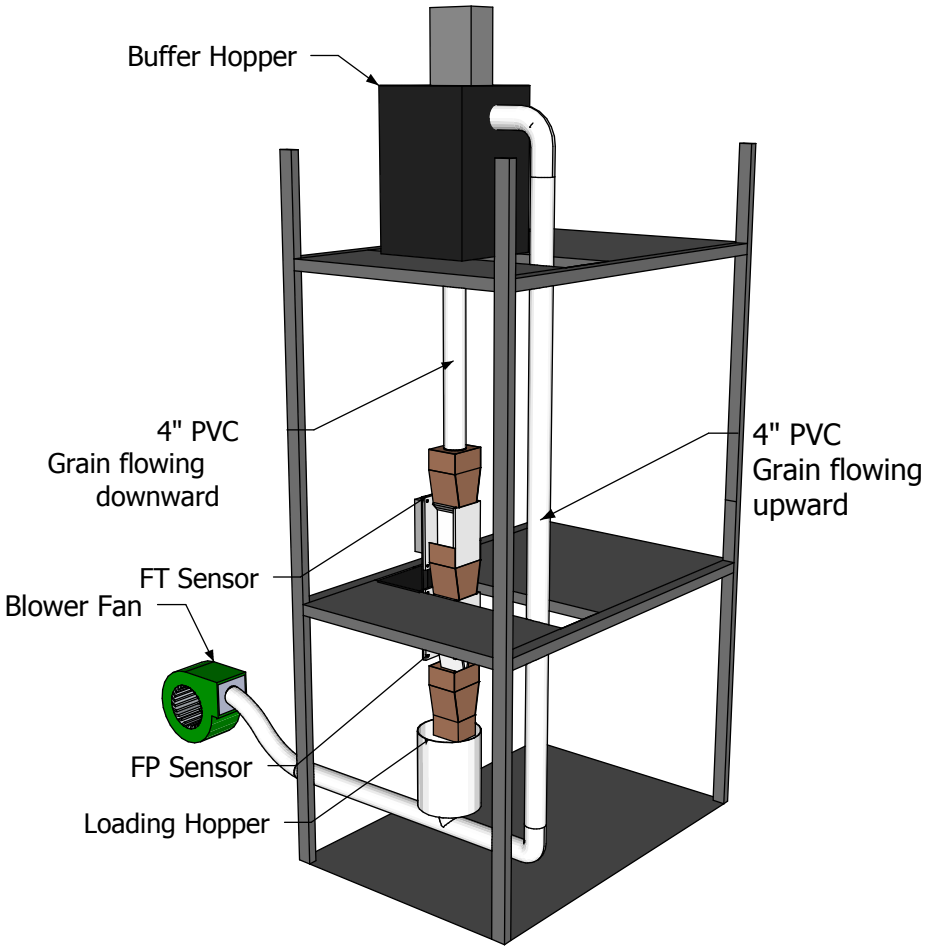

Figure 22: Schematic Diagram of Pneumatic Grain Conveyor and Sampling System.

Figure 22 shows a schematic representation of the equipment. Each sample of corn was allowed to cycle through the apparatus multiple times. Over the course of a 60 minute sampling period, the grain typically dried 0.5% due to air flow in the pneumatic conveyor.

Two moisture sensor sample cells were connected in series with a control gate below the lower sensor. The FT sensor was located above and the FP sensor was located below. As in the earlier studies, the dimensions of the FT sample cell are given in Figure 6. The electrodes of the sensors were copper on FR-4 fiberglass circuit board, protected by a 1.016 mm (0.040 in.) non-porous ceramic. For the FP sensor, the sample cell was identical to the FT. Only the sensor electrode configuration was changed; both electrodes were mounted in the same plane as shown in Figure 7. Grain flow was modulated by attaching an electrically actuated vibrator to the control gate.

Data was collected from the two sensors using instrumentation attached to a laptop running a custom LabView virtual instrument on Windows 2000 via a proprietary protocol over an RS485 physical interface (National Instruments, 1996).

The internal workings of the new instrument functioned similarly to the previous device. Pulse trains of sinusoids were sent in 12 octave steps between 10kHz and 20MHz to an electrode adjacent to the grain sample. A second electrode sensed the attenuated signal. Multiple instrumentation amplifiers fed this signal to an analog multiplier that was used to compare to an in-phase and an out-of-phase version of the original signal. These measurements were recorded directly by 10-bit analog to digital converters in the circuitry and output via the aforementioned RS485 physical interface. The raw data was stored in a tab-delimited file that could then be further analyzed.

Other factors automatically recorded by the instrumentation included a time stamp, temperatures from a sample probe, and circuit board level temperature measurement device, the RS485 sensor address, and the sensor sensitivity or gain setting.

Sampling methods

Grain moisture levels and densities were measured multiple times during each sampling period. The corn temperature was monitored continuously through the instrumentation. The protocol established was to load the sample of grain (sample weight ranging from 45 to 54 kg) into the pneumatic conveyor's lower hopper. Once a uniform and controlled flow of approximately 2.3 kg per minute was established through the sensing cells, 1.4 kg samples were collected from the lower sensor cell discharge for analysis. Additional 1.4 kg samples were taken every twenty minutes. Each time a grain sample was retrieved, the computer data acquisition system was flagged to denote exactly when the sample was drawn to provide optimum correlation to the analytical values.

Moisture measurement calculated by the standard method for wet basis moisture using a Blue-M model OV-475A-2 air-oven at 103°C for 72 hours (ASABE, 2008b). Triplicate samples of 15 grams were weighed using an AND model FX-320 electronic balance. Density measurement was performed by filling a Seedburo #204 dry quart cup with corresponding filling funnel and striking off the excess grain. Cup weights were measured with an OHAUS 800 series triple beam balance.

Data and Analysis

Unprocessed Data

The data recorded from the A4MS instrument was unprocessed in and out-of-phase data for each frequency ($Q_{inphase}$ and $Q_{outphase}$ respectively). Additionally, before and after each sample the sensors were allowed to empty out and read only air, giving a reference zero: $Z_{inphase}$ and $Z_{outphase}$. To be of analytical use, the data was translated to

dielectric constant (ε') and loss factor (ε'') values. Equations 22 and 23 illustrate the conversion.

$$\varepsilon' = \frac{Q_{inphase} \cdot Z_{inphase} + Q_{outphase} \cdot Z_{outphase}}{Z_{inphase}^{\ 2} + Z_{outphase}^{\ 2}} \tag{22}$$

$$\varepsilon'' = \frac{Q_{inphase} \cdot Z_{inphase} + Q_{outphase} \cdot Z_{outphase}}{Z_{inphase}^{\ 2} + Z_{outphase}^{\ 2}} \tag{23}$$

Figure 23 illustrates the measured dielectric constant and loss factors for the FT and FP sample cells.

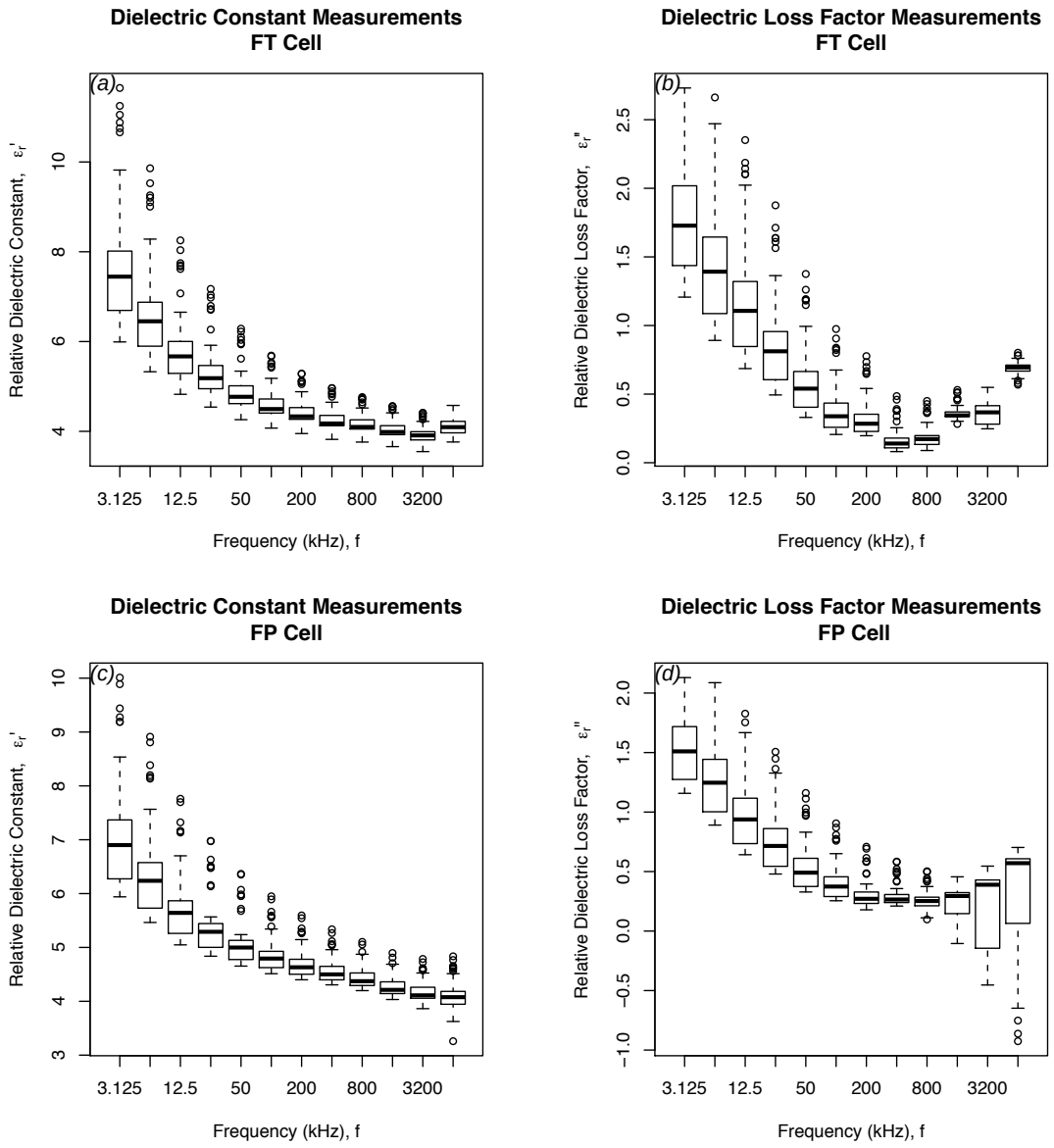

Figure 23: Measured Permittivities of Corn by Sensor Type and Frequency; (a) Dielectric Constant for FT Cell; (b) Dielectric Loss Factor for FT Cell; (c) Dielectric Constant for FP Cell; (d) Dielectric Loss Factor for FP Cell.

Differences Between FT and FP Sample Cells

Due to the physical differences between the sensor electrodes in the FT and FP sample cells, the measured complex dielectric readings were significantly different. The measured relative permittivity of the FP sample cell (sensor electrodes in single plane configuration) was approximately double that of the FT sample cell (sensor electrodes in

parallel plate configuration). Equations 24 and 25 give capacitance estimates for the FT and FP sensor cell topologies (FP sensor estimated by parallel wire configuration).

$$C = \varepsilon \cdot \frac{A}{d} \approx 4.4\varepsilon \ , \ C = \varepsilon \cdot \frac{\pi \cdot l}{2 \cdot \cosh^{-1}(\frac{d}{2r})} \approx 7.5\varepsilon \qquad (24, 25)$$

This result gave a slightly higher correction factor (0.58) than what was observed experimentally (a factor of 0.50). The difference was ascribed to the rough physical model used for the FP configuration and the experimentally observed correction was used.

What was not immediately explained was the non-linearity with which the A4MS instrument reported dielectric measurements between the two configurations. Figure 24 shows the differences between FT and FP sample cells. The non-linearity is particularly pronounced in the lowest frequencies of the dielectric constant and there is a strong moisture correlation to this effect. The topological differences between the FT and FP sample cells do have bearing on the measurement of permittivity and should be noted, particularly for the frequencies 10kHz and 20480kHz.

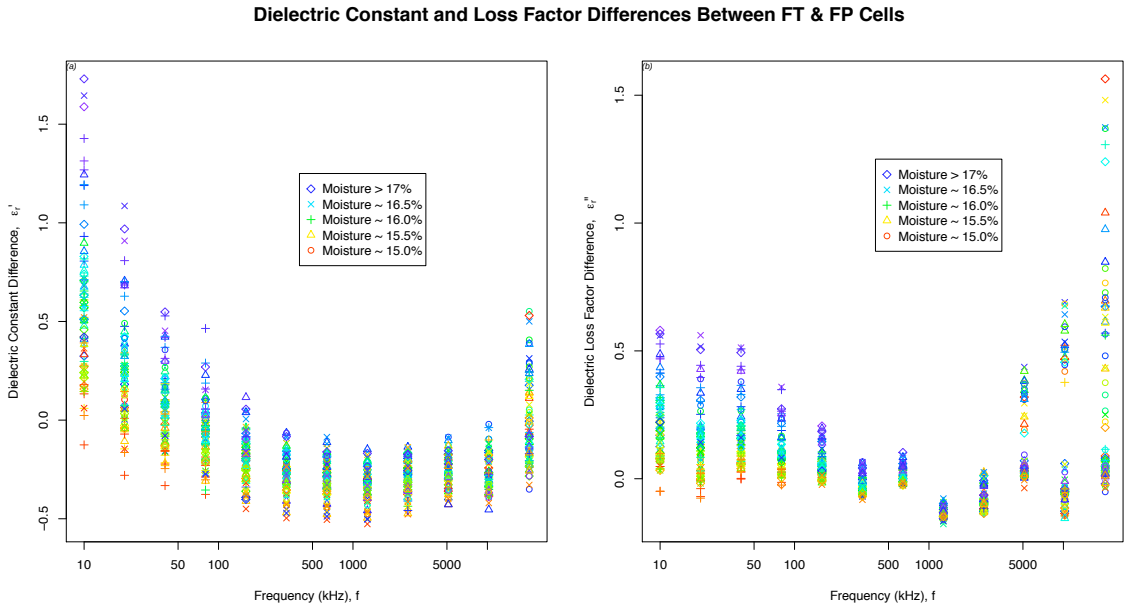

Figure 24: Permittivity measurement nonlinearities by frequency and moisture; (a) Dielectric constant differences; (b) Dielectric loss factor differences.

Moisture Dependence

As noted throughout the literature, the measure of dielectric constant is a well known predictor of moisture content in a wide variety of grains. Therefore, a proper beginning to analyze the effects would examine the models:

$$M \sim C_1 \cdot \varepsilon' + C_0 \text{ and } M \sim C_1 \cdot \varepsilon'' + C_0 \qquad (26, 27)$$

In addition to using Pearson's Correlation Coefficient to evaluate performance of models, the Standard Error of Calibration (SEC) is used:

$$SEC = \left(\frac{1}{n - p - 1} \sum_{i=1}^{n} (\Delta x_i) \right)^{1/2} \qquad (28)$$

Where n is the number of samples, p is the number of variables in the regression, and Δx_i is the difference between the value predicted by the regression and the value obtained experimentally.

For a simple linear model, best moisture prediction performance was obtained by the dielectric constant measurement at 10kHz with a SEC of 0.37% for the FT sample cell. This is shown Figure 25(a). The FP sample cell responded with an SEC of approximately six percent more over the entire frequency range. The dielectric loss factor's performance as a predictor was similar and is illustrated in Figure 25(b), and frequencies between 40kHz and 320kHz maintained SEC of less than 0.36%. Again, this was the result of the FT sample cell. The FP sample cell had larger prediction intervals, but much closer (two percent) than the dielectric constant predictor.

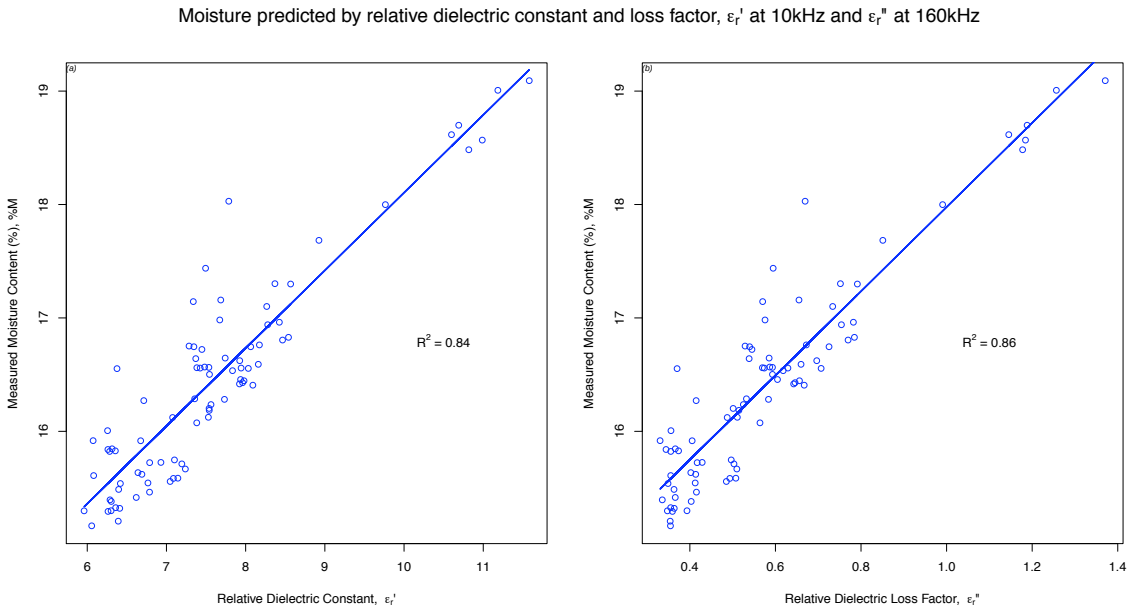

Figure 25: Linear regressions on ε' and ε'' predicting moisture; (a) Dielectric constant at 10kHz; (b) Dielectric loss factor at 160kHz.

A complete table of the fit coefficients and expected error is shown in Table 5. The additional factors of density and temperature are known variables entering into the dielectric response of grain and should be considered to improve prediction of moisture by permittivity measure.

Table 5: Fitting parameters for simple linear regression (Equations 26 and 27) of moisture against permittivity.

		FT Sensor Cell				FP Sensor Cell			
Frequency	ε' or ε"	R^2	C_0	C_1	SEC	R^2	C_0	C_1	SEC
10kHz	ε'	0.84	11.25	0.69	0.37	0.81	9.95	0.93	0.40
20kHz	ε'	0.83	10.73	0.87	0.38	0.80	9.44	1.11	0.41
40kHz	ε'	0.81	9.76	1.16	0.40	0.78	8.49	1.40	0.43
80kHz	ε'	0.78	8.63	1.48	0.43	0.75	7.26	1.72	0.46
160kHz	ε'	0.75	7.21	1.90	0.47	0.71	5.79	2.11	0.50
320kHz	ε'	0.70	5.76	2.34	0.50	0.66	4.33	2.50	0.53
640kHz	ε'	0.65	4.24	2.78	0.54	0.61	2.93	2.89	0.57
1280kHz	ε'	0.60	3.54	3.05	0.58	0.57	1.81	3.21	0.61
2560kHz	ε'	0.59	2.29	3.42	0.59	0.54	1.02	3.48	0.63
5120kHz	ε'	0.55	2.01	3.59	0.62	0.52	0.75	3.67	0.64
10240kHz	ε'	0.52	2.14	3.66	0.64	0.50	1.54	3.57	0.66
20480kHz	ε'	0.48	3.25	3.22	0.67	0.32	8.00	2.05	0.76
10kHz	ε"	0.76	12.70	2.13	0.45	0.72	11.62	3.14	0.48
20kHz	ε"	0.84	13.49	2.08	0.37	0.82	12.67	2.96	0.39
40kHz	ε"	0.85	13.82	2.28	0.35	0.85	13.33	3.19	0.36
80kHz	ε"	0.86	14.06	2.82	0.35	0.86	13.66	3.71	0.35
160kHz	ε"	0.86	14.26	3.71	0.35	0.85	13.99	4.60	0.36
320kHz	ε"	0.85	14.49	5.09	0.36	0.83	14.04	5.88	0.38
640kHz	ε"	0.83	14.29	6.67	0.38	0.79	14.14	7.45	0.42
1280kHz	ε"	0.80	14.76	10.27	0.41	0.77	13.41	10.31	0.45
2560kHz	ε"	0.60	14.62	9.91	0.58	0.33	14.73	6.48	0.76
5120kHz	ε"	0.69	10.21	17.44	0.51	0.03	16.16	1.07	0.91
10240kHz	ε"	0.22	14.44	5.71	0.82	0.01	16.37	0.20	0.92
20480kHz	ε"	0.16	10.38	8.82	0.85	0.03	16.29	0.36	0.91

Density Correction and Density Independence Methods

Density in Complete Models

The ASABE standard on dielectric properties of seeds cites Nelson's work on a calibration equation for shelled, hybrid yellow-dent field corn (ASABE, 2005). The general form of the equation is:

$$\varepsilon'_{freq} = C_0 + C_m(M-10) + (\rho_b - \overline{\rho}_b)(D_0 + D_1 M + D_2 M^2) + C_T(T-24) \qquad (29)$$

with:

$$\overline{\rho}_b = 0.6829 + 0.01422 \cdot M - 0.000979 \cdot M^2 + 0.0000153 \cdot M^3 \qquad (30)$$

ASABE cites coefficients for 20MHz, which result in the relation illustrated in Figure 26. Dielectric constant values predicted by Equation 29 were similar across all frequencies examined with the instrument; the difference in calculated versus observed dielectric

constant values would require a doubling of moisture. ASABE standard D293.2 notes that this calibration was specified for temperatures above 25°C and bulk densities below 0.74g/cm^3 (ASABE, 2005). Both of these ranges were exceeded by the data set. Noting the narrow range of this model and in particular, the non-triviality of isolating moisture from this relationship, it was determined that this calibration is not useful for the instrument being used in this study and in general for prediction of moisture. Additional density prediction functions will be discussed below.

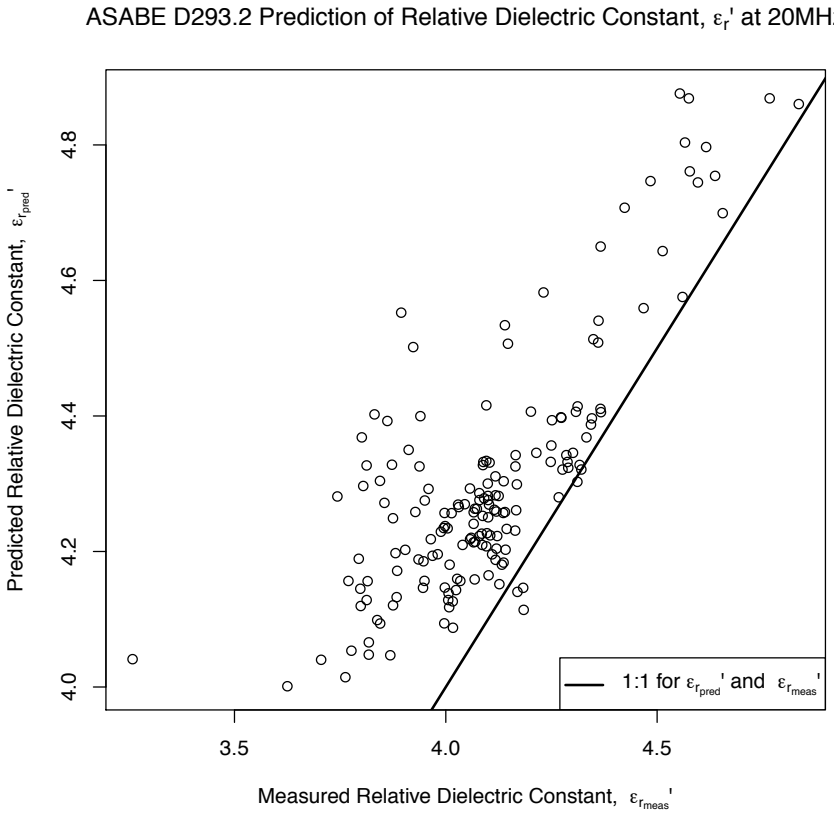

Figure 26: ASABE predicted versus measured relative dielectric constant.

Funk cites the use of the Landau and Lifshitz, Looyenga (LLL) dielectric mixture equation as a useful correction to bulk density. The model is particularly useful for differences due to moisture level, differences between samples and sample presentation:

$$\varepsilon_{corrected} = \left(\left(\varepsilon^{1/3} - 1 \right) \frac{\rho_t}{\rho_s} + 1 \right)^3 \tag{31}$$

where ρ_s and ρ_t are the sample and target bulk densities, respectively (Funk et al., 2007). Using this correction and applying the result to a linear regression of moisture and dielectric constant, the improvement is significant. Figure 27 illustrates how at certain frequencies, this density correction can improve SEC by more than 40%. This correction has an insignificant effect on the dielectric loss factor and its relationship with moisture.

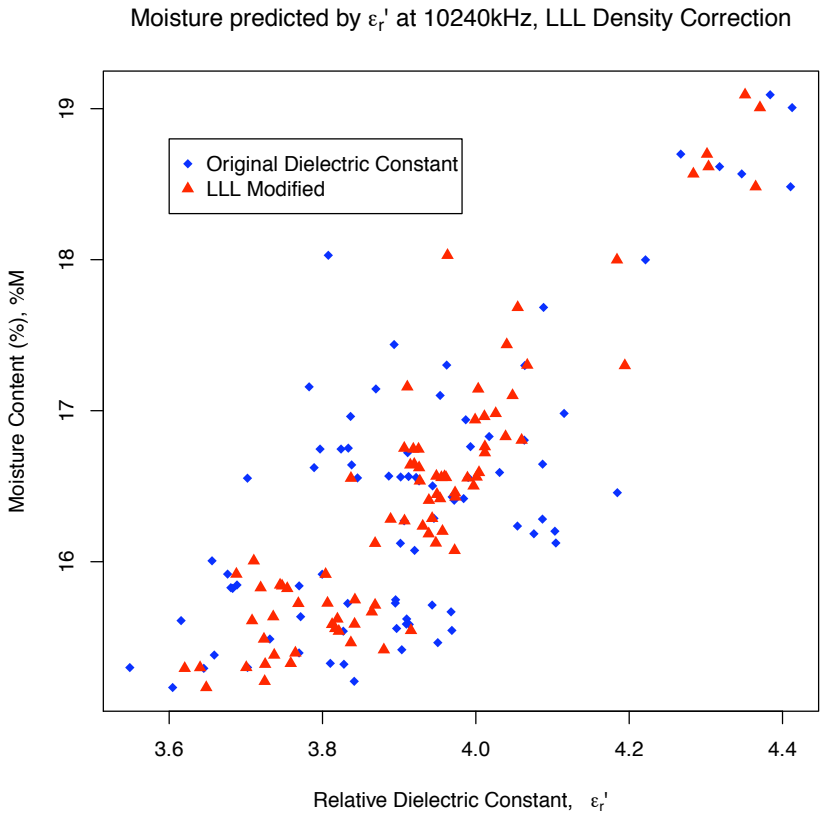

Figure 27: Landau and Lifshitz, Looyenga density correction improves overall fit of dielectric constant to moisture.

Stepping back from the complexity of these higher order models, a simple linear regression with terms for density was run to compare to the LLL method.

$$M \sim C_2 \cdot \varepsilon' + C_1 \cdot \rho + C_0 \text{ and } M \sim C_2 \cdot \varepsilon'' + C_1 \cdot \rho + C_0 \qquad (32, 33)$$

It is shown in Table 6 that performance of the linear term in Equations 32 and 33 is a marginally more robust method for density correction than the LLL method of correcting permittivity.

Another density correction method is to "shrink" the grain to a target moisture. This is accomplished by scaling the density based on the sample's proximity to the standard moisture (Equation 34).

$$\rho_{shrunk} = \rho\left(1 - \left(M_{original} - M_{shrunk}\right)\left(1 - M_{shrunk}\right)\right) \qquad (34)$$

Figure 28 shows the resulting densities compared to the original measured density. This method further reduced SEC to 0.25% for all frequencies of the dielectric constant.

Table 6: Comparison of calibration error for several density terms to moisture and permittivity regressions.

Model	SEC Means, Pooled Over All Frequencies			
ε' or ε"	M~ε	M~ε_cor†	M~ε+ρ	M~ε+ρ_s††
ε'	0.52	0.34	0.31	0.25
ε"	0.48	0.50	0.44	0.38
	† corrected by LLL method			
	†† shrunk to 15.5% equivalent			

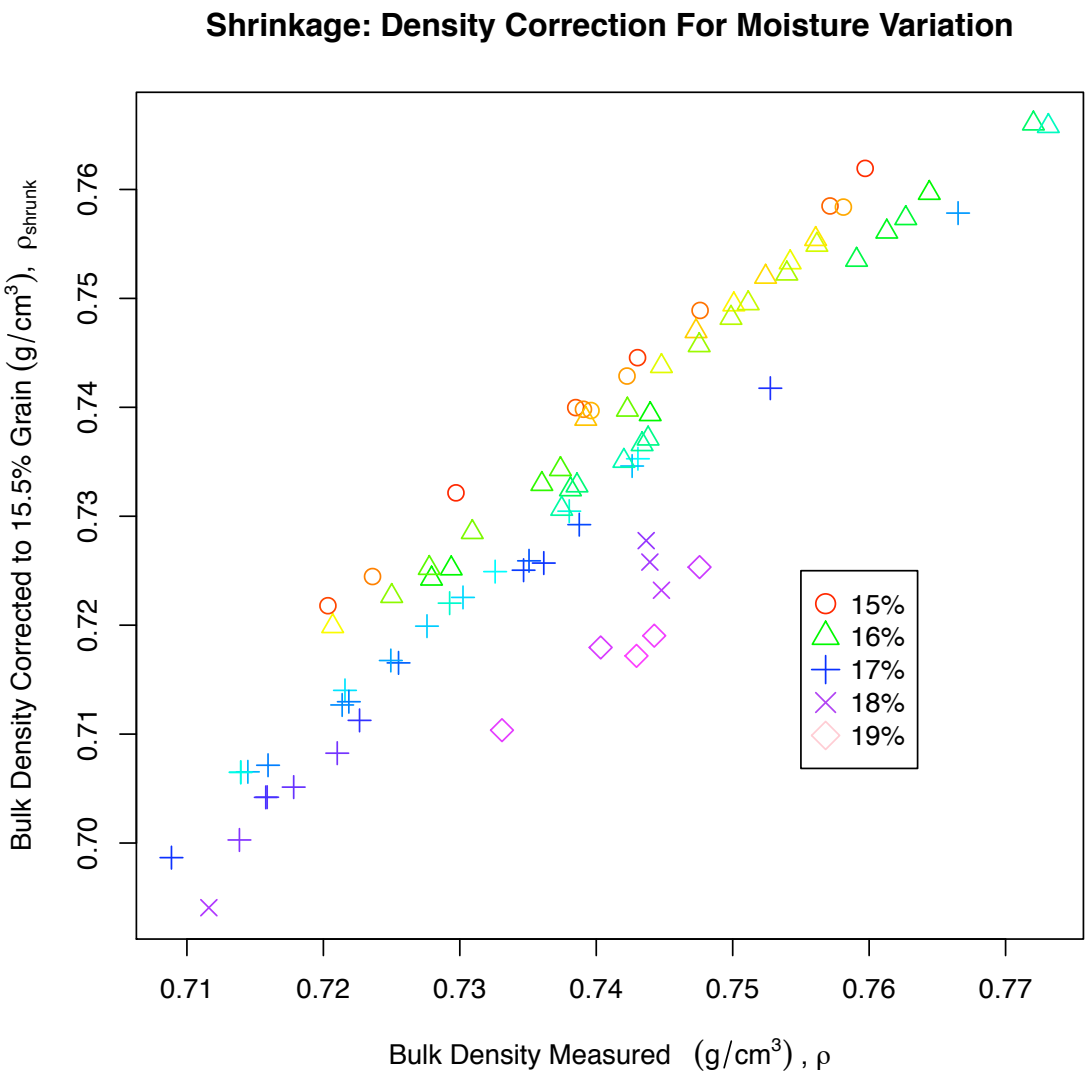

Figure 28: Bulk density of grain shrunk for linear regression moisture predictor.

Instrument's Built-In Density Independent Function

The instrument had previously used an algorithm for predicting moisture based on third order polynomial fit of the ratio between the dielectric constant at two frequencies and a linear temperature compensation factor. This model was developed as a preliminary density independent function, allowing moisture to be determined in spite of fluctuating sample bulk densities.

$$M = C_3 \cdot \Phi^3 + C_2 \cdot \Phi^2 + C_1 \cdot \Phi^1 + C_0 + C_T(25 - T) \tag{35}$$

where

$$\Phi = 10 \cdot \left(1 - \frac{\varepsilon'_{400kHz}}{\varepsilon'_{12.5kHz}}\right) \tag{36}$$

This model was non-specific for its frequency selection, so regressions as in Equation 36, were calculated for all permittivity ratios, both dielectric constant and loss factor. This model's SEC values were consistent with models requiring a known density (Table 6). However, there was still some density dependence in the model when using ratios of the dielectric loss factor for Φ. Regression with an additional linear term for density improved prediction intervals by 12% for the best ratios of dielectric loss factors. The dielectric constant ratios were improved less (3%) and such improvement could be explained by the addition of a term to the regression model. Figure 29 shows the contours of the SEC for the complete data set of predictors by frequency for the FT sample cell. This gives a general overview of what frequency ratios are most effective for the density independent function, Φ. The FP sensor cell had similar performance to the FT sensor cell in regions where Φ produced a useful result.

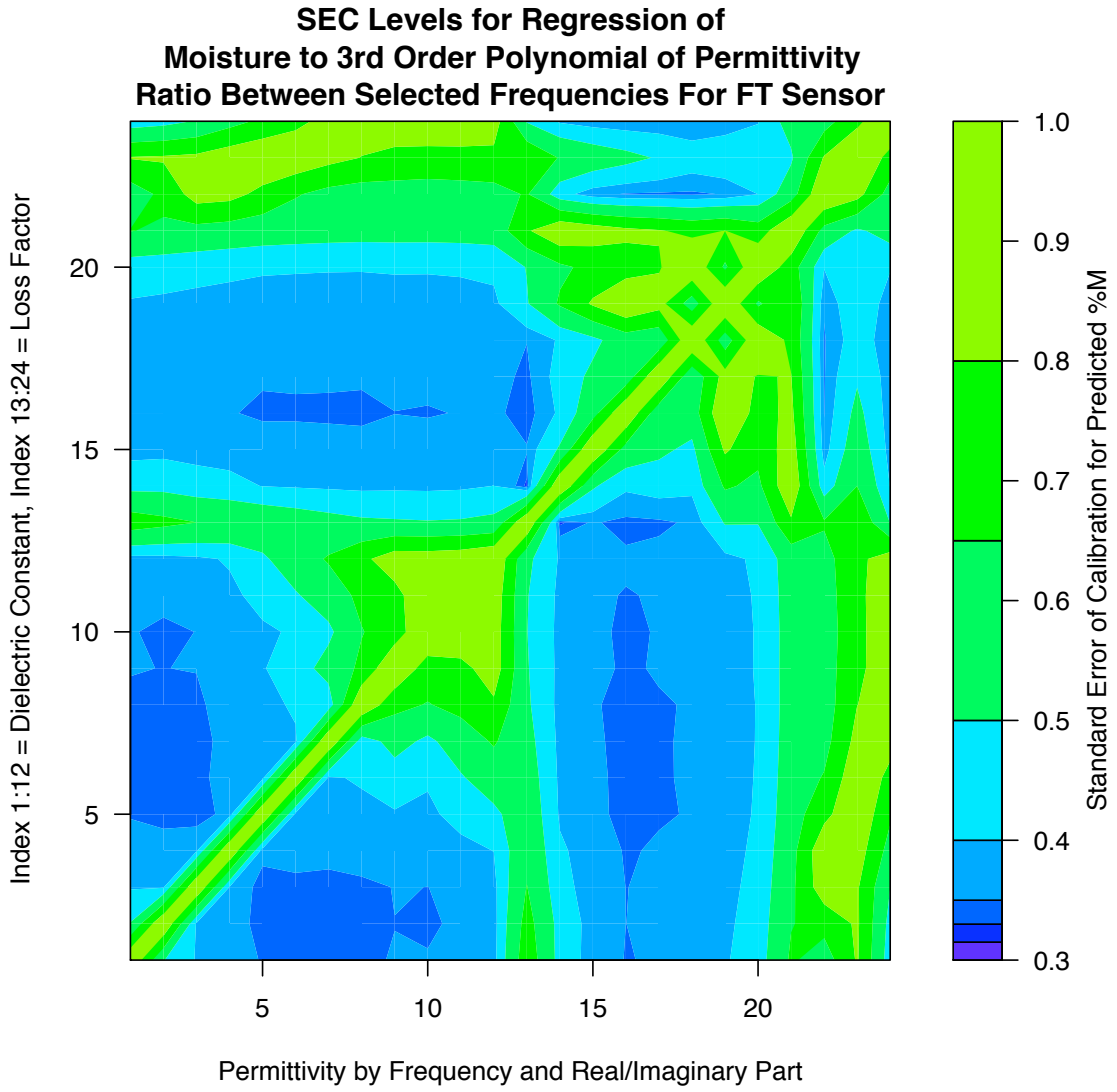

Figure 29: Contours of SEC for moisture prediction based on Φ function; by frequency and dielectric constant or loss factor.

Density Independent Models from Literature

Berbert and Stenning cite the Meyer and Schilz function as a potential density independent function (Berbert and Stenning, 1996). They note, however that the result has conflicting success in the literature at frequencies below 10GHz. The Meyer and Schilz function is another simple ratio between dielectric constant and loss factor. The

literature also illustrates that though this function is linear in small moisture ranges, over wide ranges it cannot be approximated with a linear regression.

$$\Psi_{MS} = \frac{\varepsilon' - 1}{\varepsilon''} \tag{37}$$

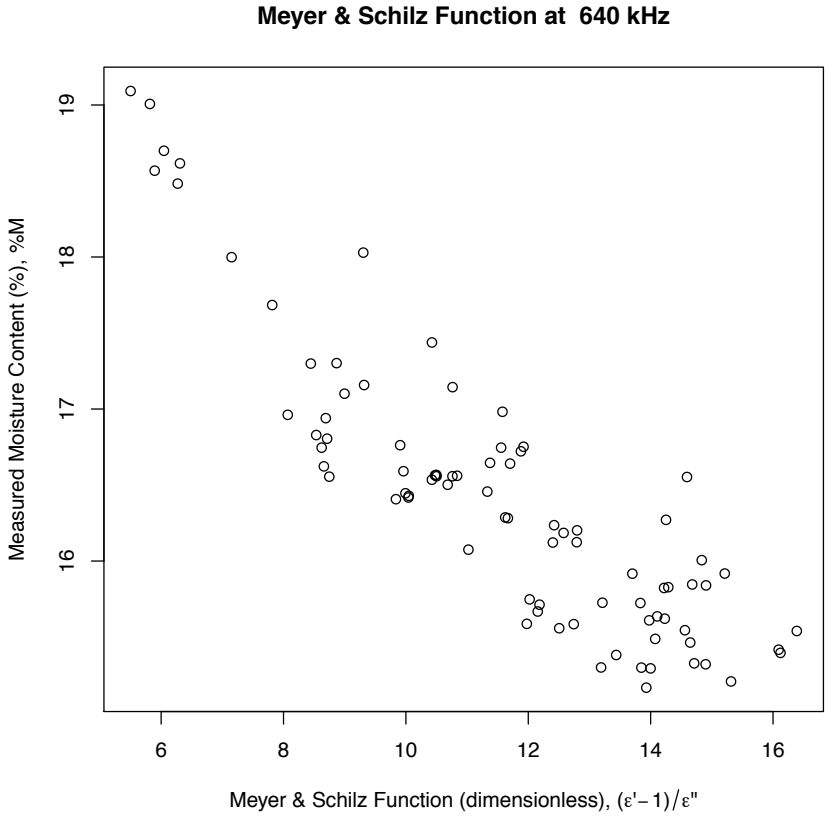

Figure 30: Meyer & Schilz function for predicting moisture independent of density.

Figure 30 illustrates this function for the FT sensor cell. The SEC of a linear model based on Figure 30 is 0.43% moisture, wet basis.

The most useful work on density independence has been done by Trabelsi, Kraszewski, and Nelson (Trabelsi et al., 1999b). Extending the ideas from the Meyer & Schilz equation, they designed a clever method for microwave frequencies where permittivities are plotted in the complex plane. The bulk densities for measured products

are divided through the dielectric constant and the dielectric loss factor. The result is a plot with a frequency dependent slope that is density dependent, shown in Figure 31.

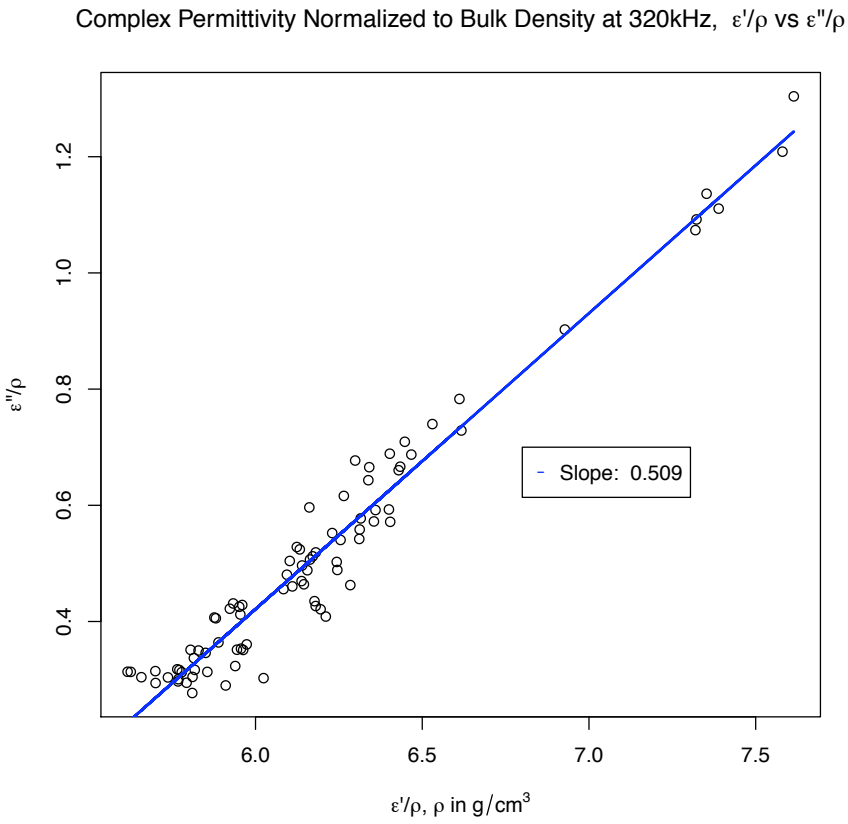

Figure 31: Complex plane plot of permittivity divided by density.

This slope gives rise to a Ψ function:

$$\Psi = \sqrt{\frac{\varepsilon'}{\varepsilon'\left(a_f \cdot \varepsilon' - \varepsilon''\right)}} \tag{38}$$

which has been shown to be a linear predictor of moisture (Trabelsi et al., 1999b). In Trabelsi's work in the microwave range, the slope of a_f over frequency was monotonic and could be fit to a simple linear regression, allowing the complete quantization of moisture at multiple frequencies. However, as is shown in Figure 32 the RF

permittivities were not consistent with this result. Instead the values of a_f increased to 160kHz and then decreased with increasing frequency.

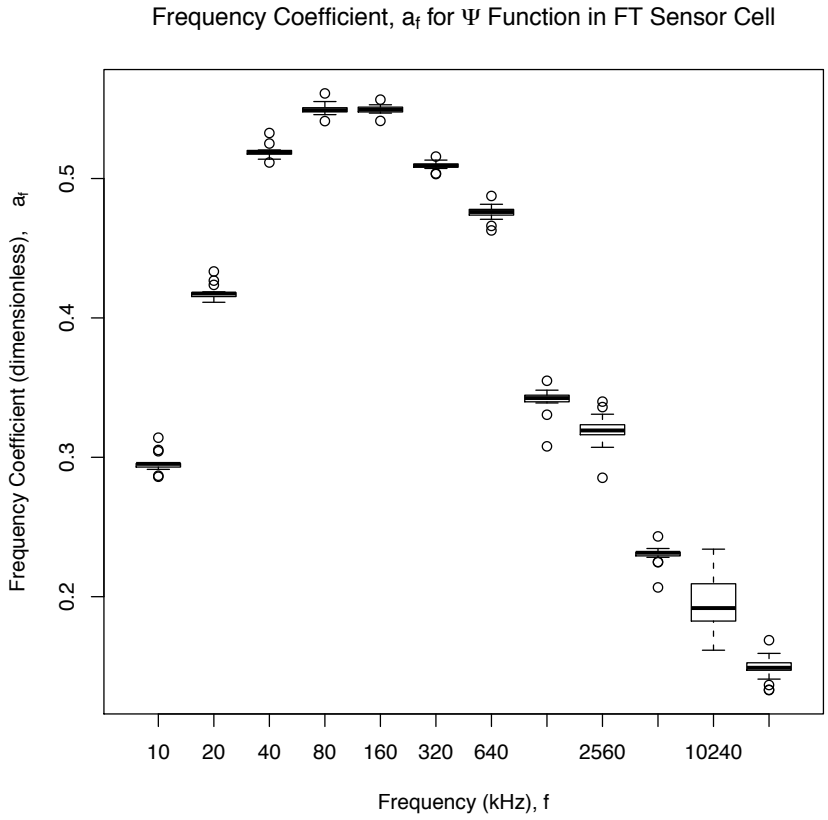

Figure 32: a_f values for Ψ function (Equation 38).

Figure 33 shows the Ψ function plotted against moisture. Table 7 shows the SEC for each frequency.

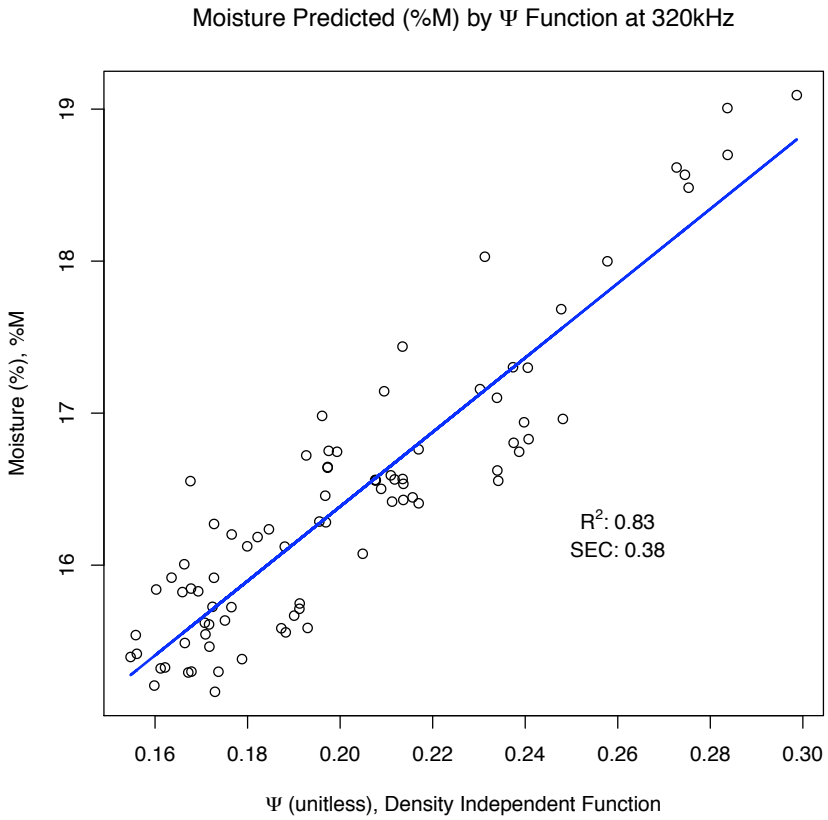

Figure 33: Results of Ψ function moisture prediction.

Table 7: SEC results of Ψ function moisture prediction for FT and FP sensor cells.

Frequency (kHz)	SEC FT	SEC FP
10	0.92	0.92
20	0.68	0.73
40	0.50	0.50
80	0.43	0.42
160	0.40	0.38
320	0.38	0.38
640	0.38	0.41
1280	0.42	0.45
2560	0.68	0.85
5120	0.69	N/A
10240	0.90	N/A
20480	N/A	N/A

Temperature Dependence

The data set had a limited temperature variation by design. The range of temperatures obtained in this data spans 7.25 to 11ºC, Figure 34. This study was not

designed to test temperature dependence. Adding temperature terms to linear regressions for this data set generally yielded statistically insignificant factors. One notable exception was the temperature dependence when the term was added to the above Ψ function. Table 8 shows values for the temperature term in the regression based on the model:

$$M \sim \Psi + T \tag{39}$$

Past research indicates that these values are appropriate (Funk, 2001; Funk et al., 2007; Trabelsi and Nelson, 2004). The cited findings have previously found a linear correction factor of approximately -0.10% moisture per degree Centigrade.

Table 8: Temperature coefficients and their significance.

Model: M~Ψ+Temperature		
Frequency (kHz)	T Estimate	T Significance
10	-0.040	7.0E-01
20	-0.057	4.4E-01
40	-0.104	5.6E-02
80	-0.116	1.2E-02
160	-0.129	2.3E-03
320	-0.113	4.9E-03
640	-0.076	6.2E-02
1280	-0.065	1.5E-01
2560	0.357	1.2E-05
5120	-0.047	5.3E-01
10240	0.213	1.5E-01
20480	N/A	N/A

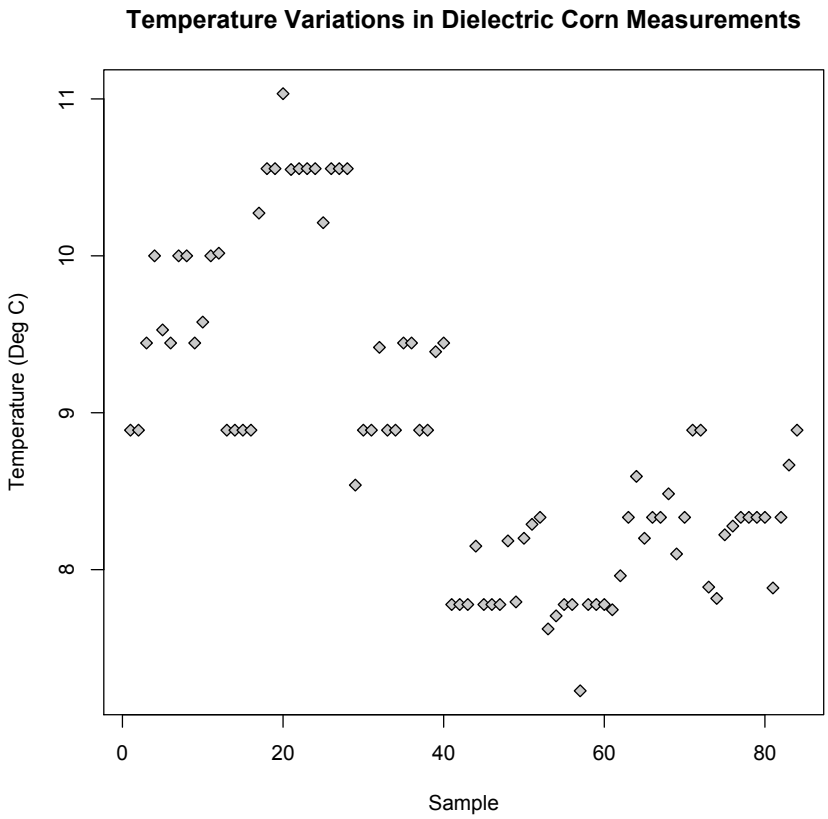

Figure 34: Temperature variations across all grain samples.

Density Dependence

Bulk density prediction by permittivity based instrumentation has been well studied (Nelson, 2006; Nelson, 2005; Trabelsi et al., 2001a; Trabelsi et al., 1999b). Density models for correlation to permittivity attempt to remove the effect that temperature and moisture have on the measured dielectric constant and loss factors either explicitly (by linear or non-linear models including these effects directly) or implicitly (using derived relationships).

Explicit Models

The most basic model for removing moisture and temperature dependence from the measured dielectric constant and loss factor is a simple linear regression. Equations 40 and 41 show this model.

$$\rho \sim C_3 \cdot M + C_2 \cdot \varepsilon' + C_1 \cdot T + C_0 \text{ and } \rho \sim C_3 \cdot M + C_2 \cdot \varepsilon'' + C_1 \cdot T + C_0 \quad (40, 41)$$

With the small temperature variations in the data, the temperature term (C_1) was not significant. A revised regression without the temperature term yielded an SEC of 0.0089 g/cm^3 (about 1.2% of the measured density).

The instrument's creator used a variation on the simple linear model. The model used is shown in:

$$\rho \sim \left(C_2 \cdot M + C_1 \cdot T + C_0\right) \cdot \log(\varepsilon') \quad (42)$$

The model performance is comparable to that of the simple linear model. SEP is shown in Table 9 (1.6% of total value). This model's performance significantly degraded with decreasing instrument frequency.

Nelson and Funk make the case for fitting the density as a linear function of the cube root of dielectric constant based on the results of the Landau and Lifshitz, Looyenga dielectric mixture equation (Funk et al., 2007; Nelson, 2005). Allowing for explicit temperature and moisture correction, the previous model becomes:

$$\rho \sim \left(C_2 \cdot M + C_1 \cdot T + C_0\right) + (\varepsilon')^{1/3} \quad (43)$$

This model had an almost identical response with an SEC of 0.0088 g/cm^3.

What is much more interesting is the result of a variation on Equation 42 (the previously used instrument model) when the logarithm is replaced with the cube root:

$$\rho \sim \left(C_2 \cdot M + C_1 \cdot T + C_0\right) \cdot (\varepsilon')^{1/3} \tag{44}$$

This model reduced the SEC to 0.0045 g/cm^3, which was a very significant reduction in error.

Psi Function and Density

Trabelsi's work on determining a density independent function included deriving a prediction of density from the same relationship (Trabelsi et al., 1999b).

$$\frac{\varepsilon'}{\rho} = a_f\left(\frac{\varepsilon''}{\rho} - k\right) \text{ solved for } \rho \text{ becomes: } \rho = \frac{a_f \cdot \varepsilon' - \varepsilon''}{a_f \cdot k} \tag{45, 46}$$

This model had very significant limitations at the limits of the frequency range tested, but SEC for the 160 to 640kHz range was ~0.015 g/cm^3.

Table 9: SEC of various density regression models.

	SEC for Density Regression Models				
Frequency (KHz)	SEC: ρ~ C2•M+C1•ε'+C0	SEC: ρ~log(ε')• (C2•M+C1•T+C0)	SEC: ρ~(ε')^(1/3)+ (C2•M+C1•T+C0)	SEC: ρ~(ε')^(1/3)• (C2•M+C1•T+C0)	SEC: ρ~(af•ε'-ε'')/k•af
10	0.0110	0.0196	0.0120	0.0071	0.2165
20	0.0100	0.0177	0.0114	0.0063	0.0430
40	0.0091	0.0155	0.0108	0.0056	0.0223
80	0.0089	0.0135	0.0102	0.0045	0.0185
160	0.0084	0.0118	0.0094	0.0041	0.0155
320	0.0080	0.0101	0.0085	0.0039	0.0148
640	0.0076	0.0089	0.0078	0.0038	0.0159
1280	0.0071	0.0088	0.0076	0.0038	0.0209
2560	0.0069	0.0079	0.0071	0.0038	0.0403
5120	0.0071	0.0078	0.0068	0.0038	0.0705
10240	0.0083	0.0087	0.0071	0.0038	0.3084
20480	0.0095	0.0090	0.0069	0.0036	0.9774
Mean	*0.0085*	*0.0116*	*0.0088*	*0.0045*	*0.1470*
					all values in g/cm^3

Conclusions

Permittivity measurements were taken at 10kHz to 20MHz in octave steps on flowing grain samples ranging from 15 to 19% wet basis moisture and 0.70 to 0.77 g/cm^3. Multiple calibrations were compared and performance evaluated for predicting moisture and density simultaneously using the measured permittivity. The apparatus in this study allowed for flowing samplings of grain leading to more robust calibrations. Though

modest in range of moistures and densities, the results of models allowing simultaneous determination of moisture content and bulk density were comparable to results in published literature.

Moisture predictions were obtained using almost any prediction model analyzed in this study as long as the frequency was selected carefully. For density, however, the cubic root model in Equation 44 is a significant improvement over existing models, halving the SEC. This study raised interesting questions about the relationship between different sensing electrode configurations in the FT and FP sensing cells. Geometry, frequency, and dielectric strength combined to influence how sensing configurations affect the observed relative permittivity. Finally, the results of these experiments have verified that many models in published literature based on microwave frequencies (300MHz to 300GHz) perform well at radio frequencies (3kHz to 300MHz).

Future work may do well to investigate some of the initial studies in this research, which examined fertilizer and soils. Necessary research would control for moisture, temperature, and density while measuring complex permittivity. Classifying by grain type and grain variety would require a large pool of controlled data (again, moisture, temperature, and density) given the findings of this research. Additional research is required to expand the newfound cubic root model (Equation 44) for density prediction to other materials beyond corn and to verify the effect of temperature on this model. Other research has suggested that VHF (30-300MHz) is more adept at higher moisture grains than LF/MF/HF (30kHz-30MHz). This could be verified by examining the response of the instrumentation from this study at higher moisture contents (20-30%, wet basis). Finally, additional moistures of grains should be examined to verify that extrapolating

models within this research to wider ranges could be done and to verify what effect this has on the error rates of said models.

References

Al-Mahasneh, M. A., S. J. Birrell, C. J. Bern and K. Adam. 2001. Measurement of Corn Mechanical Damage Using Dielectric Properties. ASABE Paper No. 01-1073. St. Joseph, Michigan: ASABE.

ASABE. 2008a. Method of Determining and Expressing Fineness of Feed Materials by Sieving. *Standards of the American Society of Agricultural and Biological Engineers* S319.4.

ASABE. 2008b. Moisture Measurement--Unground Grain and Seeds. *Standards of the American Society of Agricultural and Biological Engineers* S352.2.

ASABE. 2005. Dielectric Properties of Grain and Seed. *Standards of the American Society of Agricultural and Biological Engineers* D293.2.

Berbert, P. A. and B. C. Stenning. 1996. Analysis of density-independent equations for determination of moisture content of wheat in the radiofrequency range. *Journal of Agricultural Engineering Research* 65(4): 275.

Braun, J. D. 2003. Unpublished data. Minneapolis, Minnesota: University of Minnesota.

Debye, P. J. W. 1929. Polar molecules. New York: Chemical Catalog Company.

Funk, D. B. 2001. An investigation of the nature of the radio-frequency dielectric response in cereal grains and oilseeds with engineering implications for grain moisture meters. PhD diss. Kansas City, Missouri: University of Missouri, Kansas City. UMI No. 3010741.

Funk, D. B., Z. Gillay and P. Meszaros. 2007. Unified moisture algorithm for improved RF dielectric grain moisture measurement. *Measurement Science & Technology* 18(2007): 1004-1015.

Greer, B. D. 2002. Swept-frequency dielectric moisture and density sensor. U.S. Patent No. 6388453.

Greer, B. D. 2005. Interviewed by author. Ham Lake, Minnesota. 21 February.

Griffiths, D. J. 1981. *Introduction to electrodynamics.* Englewood Cliffs, New Jersey: Prentice-Hall.

Grimnes, S. and Ø. G. Martinsen. 2000. *Bioimpedance and bioelectricity basics.* San Diego, California; London: Academic.

Heppenstall, T. E. 1929. Process And Apparatus For Determining The Moisture Content Of Substances. U.S. Patent No. 1826247.

Hilhorst, M. A. 1998. Dielectric characterisation of soil. PhD diss. Wageningen, Gelderland, Netherlands: Wageningen Agricultural University.

Hilhorst, M. A., C. Dirksen, F. W. H. Kampers and R. A. Feddes. 2000. New dielectric mixture equation for porous materials based on depolarization factors. *Soil Science Society of America Journal* 64(5): 1581-1587.

Kraszewski, A. 1996. *Microwave aquametry: electromagnetic wave interaction with water-containing materials.* New York: IEEE Press.

Kraszewski, A. W., S. Trabelsi and S. O. Nelson. 2000. Density-independent and Temperature-compensated Moisture Content Determination in Shelled Corn by Microwave Sensing. *Sensors Update* 7(1): 51-64.

Labview. 1996. *Labview*. Ver. 4.0. Austin, Texas: National Instruments Corp.

Lawrence, K. C. and S. O. Nelson. 2000. Radiofrequency Sensing of Moisture Content in Cereal Grains. *Sensors Update* 7(1): 377-392.

Nelson, S. O. 1981. Review of factors influencing the dielectric properties of cereal grains. *Cereal Chemistry* 58(6): 487-492.

Nelson, S. O. 1992. Measurement and Applications of Dielectric-Properties of Agricultural Products. *IEEE Transactions on Instrumentation and Measurement* 41(1): 116-122.

Nelson, S. O. 1999. Dielectric properties measurement techniques and applications. *Transactions of the ASAE* 42(2): 523-529.

Nelson, S. O. 2001. Measurement and calculation of powdered mixture permittivities. *IEEE Transactions on Instrumentation and Measurement* 50(5): 1066-1070.

Nelson, S. O. 2005. Density-permittivity relationships for powdered and granular materials. *IEEE Transactions on Instrumentation and Measurement* 54(5): 2033-2040.

Nelson, S. O. 2006. Agricultural applications of dielectric measurements. *IEEE Transactions on Dielectrics and Electrical Insulation* 13(4): 688-702.

Nelson, S. O. and P. G. Bartley. 2000. Measuring frequency- and temperature-dependent dielectric properties of food materials. *Transactions of the ASAE* 43(6): 1733-1736.

Nelson, S. O., A. W. Kraszewski, C. V. K. Kandala and K. C. Lawrence. 1992. High-Frequency and Microwave Single-Kernel Moisture Sensors. *Transactions of the ASAE* 35(4): 1309-1314.

Nelson, S. O., A. W. Kraszewski, S. Trabelsi and K. C. Lawrence. 2000. Using cereal grain permittivity for sensing moisture content. *IEEE Transactions on Instrumentation and Measurement* 49(3): 470-475.

Oehlert, G. W. and C. Bingham. 2000. *MacAnova*. Ver. 4.13. Minneapolis, Minnesota: University of Minnesota.

Pozar, D. M. 1990. *Microwave engineering.* Reading, Massachusetts: Addison-Wesley.

Sacilik, K., C. Tarimci and A. Colak. 2007. Moisture content and bulk density dependence of dielectric properties of safflower seed in the radio frequency range. *Journal of Food Engineering* 78(4): 1111-1116.

Trabelsi, S., A. W. Krazsewski and S. O. Nelson. 1998. New density-independent calibration function for microwave sensing of moisture content in particulate materials. *IEEE Transactions on Instrumentation and Measurement* 47(3): 613-622.

Trabelsi, S., A. W. Krazsewski and S. O. Nelson. 1999a. Unified calibration method for nondestructive dielectric sensing of moisture content in granular materials. *Electronics Letters* 35(16): 1346-1347.

Trabelsi, S., A. W. Kraszewski and S. O. Nelson. 1999b. Determining physical properties of grain by microwave permittivity measurements. *Transactions of the ASAE* 42(2): 531-536.

Trabelsi, S., A. W. Kraszewski and S. O. Nelson. 2001a. Microwave dielectric sensing of bulk density of granular materials. *Measurement Science & Technology* 12(12): 2192-2197.

Trabelsi, S., A. W. Kraszewski and S. O. Nelson. 2001b. Universal calibration method for microwave moisture sensing in granular materials. *Transactions of the ASAE* 44(3): 731-736.

Trabelsi, S. and S. O. Nelson. 2004. Temperature dependence of bound water dielectric behavior in grain. *Instrumentation and Measurement Technology Conference, 2004. IMTC 04.* In *Proceedings of the 21st IEEE* 1; 166-69 Vol.1.

Trabelsi, S. and S. O. Nelson. 2007. Influence of nonequilibrated water on microwave dielectric properties of wheat and related errors in moisture sensing. *IEEE Transactions on Instrumentation and Measurement* 56(1): 194-198.

Von Hippel, A. R. 1954. *Dielectric materials and applications.* Cambridge: Published jointly by the Technology Press of M. I. T. and Wiley, New York.

Webb, A. R. 2002. *Statistical pattern recognition.* 2nd ed. West Sussex, England; New Jersey: Wiley.